1 **Contrasting patterns of genetic admixture explain the phylogeographic history of**

2 **Iberian high mountain populations of midwife toads**

3

4 Federica Lucati[1,2]*, Alexandre Miró[2], Jaime Bosch[3,4], Jenny Caner[2], Michael Joseph

5 Jowers[5,6], Xavier Rivera[7], David Donaire-Barroso[8], Rui Rebelo[1] and Marc Ventura[2]*

6

7 [1] Centre for Ecology, Evolution and Environmental Changes (cE3c), Faculty of
8 Sciences, University of Lisbon, Lisbon, Portugal
9
10 [2] Center for Advanced Studies of Blanes (CEAB-CSIC), Blanes, Catalonia, Spain
11
12 [3] Museo Nacional de Ciencias Naturales-CSIC, Madrid, Spain
13
14 [4] Research Unit of Biodiversity - CSIC/UO/PA, Universidad de Oviedo, Mieres, Spain
15
16 [5] Centro de Investigação em Biodiversidade e Recursos Genéticos (CIBIO/InBIO),
17 Universidade do Porto, Campus Agrario De Vairão, Vairão, Portugal
18
19 [6] National Institute of Ecology (NIE), Seocheon, Republic of Korea
20
21 [7] Catalan Society of Herpetology, Leonardo Da Vinci square 4-6, Barcelona, Catalonia,
22 Spain
23
24 [8] Calle Mar Egeo 7, Jerez de la Frontera, Cadiz, Spain
25
26

27 * Corresponding authors

28 E-mail: federicalucati@hotmail.com (FL)

29 E-mail: ventura@ceab.csic.es (MV)

Abstract

Multiple Quaternary glacial refugia in the Iberian Peninsula, commonly known

as "refugia within refugia", allowed diverging populations to come into contact and

admix, potentially boosting substantial mito-nuclear discordances. In this study, we

employ a comprehensive set of mitochondrial and nuclear markers to shed light onto

the drivers of geographical differentiation in Iberian high mountain populations of

the midwife toads *Alytes obstetricans* and *A. almogavarii* from the Pyrenees, Picos de

Europa and Guadarrama Mountains. In the three analysed mountain regions, we

detected evidence of extensive mito-nuclear discordances and/or admixture

between taxa. Clustering analyses identified three major divergent lineages in the

Pyrenees (corresponding to the eastern, central and central-western Pyrenees),

which possibly recurrently expanded and admixed during the succession of glacial-

interglacial periods that characterised the Late Pleistocene, and that currently follow

a ring-shaped diversification pattern. On the other hand, populations from the Picos

de Europa mountains (NW Iberian Peninsula) showed a mitochondrial affinity to

central-western Pyrenean populations and a nuclear affinity to populations from the

central Iberian Peninsula, suggesting a likely admixed origin for Picos de Europa

populations. Finally, populations from the Guadarrama Mountain Range (central

Iberian Peninsula) were depleted of genetic diversity, possibly as a consequence of a

recent epidemic of chytridiomycosis. This work highlights the complex evolutionary

50 history that shaped the current genetic composition of high mountain populations,

51 and underscores the importance of using a multilocus approach to better infer the

52 dynamics of population divergence.

53

Introduction

55   Patterns of population structure and genetic divergence within species

56 primarily result from their evolutionary history and contemporary dispersal

57 capability, and these processes are in turn responsible of generating specific

58 phylogeographic signatures [1]. The description of these signatures return valuable

59 information on the mechanisms underlying spatial patterns of contemporary genetic

60 diversity and structure, and this knowledge can ultimately help in the conservation

61 and management of species and populations under global change [2].

62   Organisms with limited dispersal capacity and a typically allopatric type of

63 speciation, such as many amphibians, generally present complex genetic signals at

64 lineage borders resulting in reticulate patterns [3-5]. A number of mechanisms are

65 involved in the generation of reticulate patterns in phylogeography, among them

66 contact zones, hybridisation and introgression [6]. Such mechanisms, among others,

67 may result in the formation of discordant patterns of variation among genetic

68 markers (i.e. mito-nuclear discordances, e.g. [4, 7, 8]). As a consequence, these

69   discordances represent a powerful source of insights into the evolutionary history of

70   species.

71   Quaternary climatic fluctuations had a major impact on worldwide biotas and

72   organisms, reshaping the distribution of species and modelling their genetic structure

73   [9, 10]. In Europe, it is acknowledged that the Iberian Peninsula has served as one of

74   the most important refugia for temperate species during periods of climatic

75   instability [11]. Growing evidence has revealed that in this region, characterized by a

76   great variety of climatic and ecological conditions, multiple isolated refugia were

77   present, which promoted genetic diversification and ultimately determined complex

78   phylogeographic patterns in a number of taxa (the "refugia within refugia" scenario;

79   [11, 12]). In this context, Iberian mountain ranges played a major role in favouring

80   survival throughout the Pleistocene. The Iberian Peninsula has several mountain

81   ranges that permitted flexibility and survival of populations through altitudinal shifts,

82   allowing for movements up or down the mountains in search of suitable

83   microclimates as the temperatures changed [11, 13]. Nevertheless, there is a lack of

84   knowledge on the phylogeographic history of European species with Iberian

85   distribution to understand the role of glacial refugia throughout the different

86   mountain regions within Iberia [11].

87   The common midwife toad (*Alytes obstetricans*) is a small anuran widely

88   distributed in central and western Europe. It is a common species that inhabits a wide

89   variety of habitats between sea level and 2 400 meters above sea level (m.a.s.l.) in

90   the Pyrenees [14, 15]. Major threats to the species are related to habitat loss and

91   fragmentation through pollution, commercial and agricultural development,

92   introduction of non-native species, and more recently emergent diseases such as

93   chytridiomycosis, which is caused by the chytrid fungus *Batrachochytrium*

94   *dendrobatidis* (*Bd*) [14-16]. *Bd* has led to episodes of mass mortality in *A.*

95   *obstetricans*, which is known to be highly susceptible to the pathogen [16-18].

96   Furthermore, fatal outbreaks of chytridiomycosis in Iberia were more frequent at

97   higher elevations [19].

98   *Alytes obstetricans* represents an excellent biological system to study

99   phylogeographic patterns derived from post-glacial expansion, such as contact zones

100   and hybridisation. The species shows strong genetic subdivisions in the Iberian

101   Peninsula, indicative of past population isolation [20]. Until recently, *A. obstetricans*

102   was defined by six divergent and geographically structured mtDNA haplogroups

103   (named A to F; [20, 21]), delineating as many genetic lineages that probably

104   interbreed in zones of secondary contact (Fig 1). Each of the six mitochondrial

105   lineages corresponded to a unique nuclear microsatellite clade, except for lineage B

106   that harboured two distinct microsatellite clusters [22]. More recently, the

107   subspecies *almogavarii* (mtDNA lineages E-F) was proposed as an incipient species

108   (i.e. *A. almogavarii*; [23]) by RAD-sequencing analysis, and mtDNA lineage E described

109   as a novel subspecies (*A. a. inigoi*) [24].

110

111 **Fig 1. Geographic location of sampling sites for *Alytes obstetricans/almogavarii*.**

112 The three analysed mountain regions are circled in white. In the Pyrenees, dashed

113 lines delimit the three geographic sections (eastern, central and western Pyrenees).

114 For population codes and further information on sampling sites see S1 Table. The

115 inset map shows the distribution of the main lineages: orange - ND4 haplogroups E-F

116 (*A. almogavarii*), yellow - ND4 haplogroup B (*A. o. obstetricans*), blue - ND4

117 haplogroup A (*A. o. pertinax*), red - ND4 haplogroup C (*A. o. boscai*), green - ND4

118 haplogroup D (*A. o. boscai*), black - unclear (adapted from Dufresnes and Martínez-

119 Solano [23]).

120

121

122   Previous studies revealed a complex scenario of relationships and admixture

123 between lineages of *A. obstetricans/almogavarii*, evidencing the existence of contact

124 and hybrid zones at some lineage borders [20, 23, 25, 26]. Yet, there has been little

125 attempt on identifying the causes and consequences of such admixture.

126 Furthermore, none of these studies was specifically focused on high mountains,

127 which are well-known hotspots of genetic diversity and have been shown to play a

128 considerable role in separating well-differentiated intraspecific clades in numerous

129 species (e.g. [4, 27]). Here, we employ a multilocus approach combined with

130 comprehensive sample collection across four of the defined mtDNA genetic lineages

131 to analyse the geographical differentiation in *A. obstetricans/almogavarii*, placing

132   special focus on three high mountain regions in the Iberian Peninsula: Pyrenees, Picos

133   de Europa and Guadarrama Mountain Range. Specifically, we aimed to (1) describe

134   finer-scale geographical patterns of genetic diversity and structure in high mountain

135   populations of *A. obstetricans/almogavarii*, compare different scenarios of

136   population divergence and explore the role of glacial refugia; (2) identify putative

137   contact zones and assess patterns of admixture; and (3) better delineate the

138   geographic distribution of major genetic lineages. We also provide deeper analyses

139   on the genetic status of populations that have been hit by a recent chytridiomycosis

140   outbreak. To this end, we combined DNA sequence (mitochondrial and nuclear) and

141   microsatellite data for the first time in an *A. obstetricans/almogavarii* study. Thus,

142   herein we provide new insights on the recent evolutionary history and the present

143   processes that have shaped and are currently shaping Iberian populations of *A.*

144   *obstetricans/almogavarii*.

145

Materials and Methods

Sampling and DNA extraction

148   Sampling was conducted mainly in the period 2009–2018 across northern and

149   central Iberian Peninsula, as it is known to host most of the genetic diversity of the

150   species [20, 22]. We paid special emphasis on three mountain regions: Pyrenees,

151   Picos de Europa mountains (Cantabrian Mountains, NW Iberian Peninsula) and

152   Guadarrama Mountain Range (central Iberian Peninsula), although we also took

153   some additional samples from neighbouring lowland localities (Fig 1, Tables 1 and

154   S1). We sampled 51 sites in the Pyrenees (1010–2447 m.a.s.l.), 13 in Picos de Europa

155   (1120–2079 m.a.s.l.), nine in Guadarrama Mountains (1527–1980 m.a.s.l.), and 32

156   sites in lowland areas (52–992 m.a.s.l.), totalling 890 individuals from 105 sampling

157   sites (Table 1). Lowland populations were grouped according to their geographic

158   proximity to the analysed mountain regions (Table 1). A subset of samples was used

159   in a previous study [18].

160

161   **Table 1. Genetic diversity parameters as estimated from microsatellites for each**

162   **analysed mountain region and corresponding lowland areas.**

	Alt.	N_{pops}	N	Na	Ar	PAAr	H_O	H_E	N_e	ND4 haps
Eastern Pyrenees	1010-2406	17	144	13.47	5.310	0.780	0.480	0.701	14-51	28(F)
Eastern Pyrenees – lowland	62-948	9	21	8.588	5.310	0.830	0.460	0.691	-	11(F)
Central Pyrenees	1211-2003	9	52	10.82	5.130	0.920	0.401	0.651	68	15(E), 4(B)
Central Pyrenees – lowland	567	1	2	-	-	-	-	-	-	2(E)
Central-western Pyrenees	1043-2447	25	284	14.12	5.240	0.990	0.377	0.708	12-84	61(B)
Central-western Pyrenees – lowland	992	1	1	-	-	-	-	-	-	1(B)
Picos de Europa	1120-2079	13	202	12.71	5.740	1.080	0.595	0.789	19-160	31(B)
Picos de Europa – lowland	464-928	3	3	-	-	-	-	-	-	3(B)
Guadarrama	1527-1980	9	112	7.529	3.940	0.580	0.442	0.613	5-15	25(A)
Guadarrama – lowland	52-830	18	57	14.53	6.580	1.080	0.620	0.805	70	36(A), 2(B)

163

164   Alt. – altitudinal range, N_{pops} – number of populations, N – sample size for

165   microsatellites, Na – mean number of alleles, Ar – allelic richness standardized for

166   sample size, PAAr – rarefied private allelic richness standardized for sample size, H_O –

167   observed heterozygosity, H_E – expected heterozygosity, N_e – range of effective

168   population size, ND4 haps – occurrence and code (in parentheses) of mitochondrial

169   ND4 haplogroups identified in each deme.

170

171   Tissue samples were collected via tail clipping in the case of larvae and toe

172   clipping in the case of adults. Samples were stored in absolute ethanol and

173   maintained at -20 °C. Genomic DNA was extracted using QIAGEN DNeasy Blood &

174   Tissue Kit (Qiagen, Hilden, Germany) according to the manufacturer's protocol, or

175   following the HotSHOT method [28], in a final volume of 100 µl for toe clips and 250

176   µl for tail clips.

177

178   Nuclear and mitochondrial genes sequencing

179   We amplified five gene regions, including four mitochondrial fragments

180   (cytochrome *b* gene – cyt-*b*; 12S rRNA gene – 12S; 16S rRNA gene – 16S; and NADH

181   dehydrogenase subunit 4 gene and adjacent tRNAs – ND4) and one nuclear gene (β-

182   fibrinogen intron 7 – β-fibint7). Details on primers used and amplification conditions

183   are provided in S1 Appendix.

184   Resulting sequences were aligned using the ClustalW algorithm in MEGA 7

185   with default settings [29]. Phasing of the nuclear intron β-fibint7 was performed

186   following Gonçalves et al. [20]. Briefly, we used the program SeqPHASE [30] to format

187   the input files, and the Bayesian algorithm implemented in PHASE 2.1.1 [31, 32] to

188   infer phased haplotypes. PHASE was run three times using default values, to check

189   for consistency of haplotype estimation across runs.

190

Microsatellite screening and estimation of genetic diversity

191   878 individuals from 102 localities were screened for 17 previously

192 characterised microsatellite loci combined in five multiplexes [21]. Fragments were

193 sized with LIZ-500 size standard and binned using Geneious 11.0.5 [33].

194   The presence of potential scoring errors, large allele dropout and null alleles

195 was tested using MICRO-CHECKER 2.2.3 [34]. We tested for linkage disequilibrium

196 between loci and for departures from Hardy-Weinberg equilibrium (HWE) in each

197 population and for each locus using GENEPOP 4.2 [35]. The Bonferroni correction was

198 applied to adjust for multiple comparisons (α = 0.05; [36]).

199   Genetic diversity parameters were calculated for populations with $\geq$ five

200 genotyped individuals and for each analysed mountain region and corresponding

201 lowland areas. Observed (H_O) and expected heterozygosity (H_E) and mean number of

202 alleles (Na) were obtained with GenAlEx 6.5 [37]. Allelic richness (Ar) standardized for

203 sample size and rarefied private allelic richness (PAAr – calculated only at the genetic

204 cluster level) were calculated in HP-RARE 1.1 [38]. We estimated the inbreeding

205 coefficient (F_{IS}) within each population with GENETIX 4.05.2 [39].

206

Phylogenetic analyses

207   For ND4, we estimated genealogic relationships among haplotypes using

208 Haploviewer [40]. The optimal nucleotide-substitution model was determined by

211   jModelTest 2.1.3 [41], under the Akaike Information Criterion (AIC). The phylogeny

212   was estimated with RAxML 7.7.1 [42] using a Maximum Likelihood (ML) approach.

213   The program was run with a gamma model of rate heterogeneity and no invariant

214   sites (GTRGAMMA), applying 1 000 bootstrap replicates. The best tree was selected

215   for haplotype network construction in Haploviewer, based on all sequences retrieved

216   from GenBank and this study. Furthermore, genetic diversity parameters, namely

217   number of haplotypes (H) and polymorphic sites (S), as well as haplotype (Hd) and

218   nucleotide (Π) diversity indices, were estimated for the whole dataset and for each

219   analysed mountain region and corresponding lowland areas using DnaSP 6.11.01

220   [43].

221   In order to describe the affinities of the different genetic lineages described in

222   *A. obstetricans/almogavarii*, we constructed a species tree with the five partially

223   sequenced genes using the multispecies coalescent approach in *BEAST, as

224   implemented in BEAST 2.6.2 (S1 Fig) [44]. The substitution model for each marker

225   was determined by jModelTest. We set a strict molecular clock model and a Yule

226   speciation prior. The clock and tree models for mtDNA markers were linked. We

227   defined five groups in *A. obstetricans/almogavarii*, corresponding to the four main

228   population lineages identified in the haplotype network (A, B, E, F) and further

229   subdividing lineage B into two groups (central-western Pyrenees and Picos de

230   Europa; see Results). Since *BEAST does not take into account the possibility of gene

231   flow between lineages, samples from localities where more than one mtDNA

11

232   haplogroup was found were excluded from the analysis [20]. Samples of *A. maurus*

233   were used as outgroup. Two independent MCMC chains were run for 200 million

234   generations each, sampling trees and parameter estimates every 5 000. Tracer 1.6

235   [45] was used to check for stationarity and convergence of MCMC chains. A

236   maximum clade credibility tree was constructed in TreeAnnotator 2.6.2 and

237   visualized using FigTree 1.4.3 (http://tree.bio.ed.ac.uk/software/figtree), discarding

238   the first 10% generations as burn-in, while the node heights were set to mean

239   heights.

240

Genetic structure

242   For microsatellites, population structure was inferred using different

243   approaches (S1 Fig): a) a Discriminant Analysis of Principal Components (DAPC) and a

244   Principal Component Analysis (PCA), using the ADEGENET package 2.1.1 [46] in R

245   3.5.1 [47]; b) a Bayesian cluster analysis implemented in STRUCTURE 2.3.4 [48]; c) a

246   neighbour-joining (NJ) tree using the program POPTREEW [49]; and d) a spatial-based

247   clustering approach implemented in the R package Tess3R 1.1.0 [50], which

248   incorporates geographic coordinates in estimating sample ancestry coefficients.

249   Details on models and parameters used are outlined in S1 Appendix.

250   To further explore the genetic differentiation between the defined genetic

251   units, we calculated pairwise F_{ST} for both ND4 and microsatellites. Computations

252   were performed in Arlequin 3.5.2.2 [51] in the case of ND4 and in GenAlEx in the case

253   of microsatellites, with 1 000 permutations to assess statistical significance. Similarly,

254   to partition genetic variability at different hierarchical levels (among genetic clades,

255   among populations within clades and within populations), we conducted an analysis

256   of molecular variance (AMOVA) as implemented in Arlequin, using 10 000

257   permutations to assess significance of variance components [52]. To better

258   understand the spatial pattern of population differentiation detected in the Pyrenees

259   (see Results), we correlated genetic distances (F_{ST}) of Pyrenean populations either

260   with the Euclidean distance among populations, and with the geographic distance

261   suggested by PCA analysis, which followed a ring-like pattern around the Pyrenean

262   chain assuming no direct gene flow across the central Pyrenean axis (see e.g. [53] for

263   a similar approach). The analysis was performed in GenAlEx with 1 000 permutations,

264   including only populations with ≥ five genotyped individuals (N = 29).

265

Effective population size

267   The sibship assignment method implemented in Colony 2.0.6.5 was used to

268   calculate the effective population size (N_e) of populations with ≥ 15 genotyped

269   individuals (S1 Fig) [54]. This software uses a maximum likelihood method to conduct

270   parentage and sibship inference to estimate N_e and can accommodate null alleles and

271   other genotyping errors. The program was run with the parameters specified in

272   Lucati et al. [55]. During sampling care was taken to minimize the effects of sampling

273   individuals belonging to the same clutch, by collecting samples from several spots

274   within the same sampling site.

275

Demographic history

277   The approximate Bayesian computation (ABC) approach, as implemented in

278   the software DIYABC 2.1.0 [56], was used to reconstruct the history of divergence

279   among the genetic lineages identified in *A. obstetricans/almogavarii*. Only high

280   mountain populations were included in the analysis, as we were interested in

281   understanding the evolutionary history of the three high mountain areas described

282   above (S1 Fig). We grouped populations into five groups according to their

283   geographic location. We also incorporated the information from previous studies

284   dealing with the phylogenetics and population structure of the different subspecies,

285   which point to a shared origin between populations from the central and eastern

286   Pyrenees (mitochondrial ND4 haplogroups E and F in Gonçalves et al. [20] and

287   microsatellite clusters F1n and F2n in Maia-Carvalho et al. [22]): populations from the

288   Picos de Europa mountains (PEU) and the central-western Pyrenees (CWPY;

289   corresponding to subspecies *A. o. obstetricans*) formed two separate groups,

290   whereas populations from the central Pyrenees (CPY), eastern Pyrenees (EPY;

291   corresponding to the putative incipient species *A. almogavarii*) and Guadarrama

292   Mountains (GUA; corresponding to subspecies *A. o. pertinax*) were subdivided into

293   three groups. We generated five different scenarios (Fig 2a): (1) null model with all

294   groups diverging simultaneously from a common ancestor, except for lineage CPY

295   that originates from EPY; (2) sequential splitting model directly following results from

296   STRUCTURE and DAPC analyses, where on the one hand populations from the

297   Pyrenees, and on the other GUA and PEU populations share a common origin; (3)

298   similar to the second one, but predicts a common origin of PEU and CWPY

299   populations, as suggested by ND4 haplotype network; (4) same as the previous

300   scenario, with a common origin between populations belonging to ND4 haplogroups

301   A and B, as suggested by *BEAST analysis; and (5) where the PEU lineage was created

302   by admixture of CWPY and GUA populations. We performed the computations both

303   combining microsatellites and ND4 data, and separately for microsatellites. Further

304   details on model specifications and run parameters are outlined in S1 Appendix and

305   S2 Table.

306

307   **Fig 2. Phylogeographic scenarios tested in DIYABC and best supported models.** (a)

308   Scenarios tested in DIYABC considering the three analysed high mountain areas. (b)

309   The best supported scenarios, namely number 2 when considering only

310   microsatellites and number 5 when considering both mtDNA (ND4) and microsatellite

311   markers, with the estimated divergence times (t1 – t3) of each split. Population

312   groups were defined on the basis of their geographic distribution and the results

313   from clustering analyses: eastern Pyrenees (EPY, orange), central Pyrenees (CPY,

314   grey), central-western Pyrenees (CWPY, pink), Picos de Europa mountains (PEU,

315   yellow), and Guadarrama Mountain Range (GUA, blue).

316

Results

Sequence variation and genetic diversity

319   The nuclear DNA alignment (β-fibint7) included 20 sequences of 605 bp, while

320   for the mitochondrial dataset we obtained 219 sequences of 654 bp for ND4, 40

321   sequences of 325 bp for cyt-*b*, 42 sequences of 341 bp for 12S, and 40 sequences of

322   579 bp for 16S (S1 Table). With regard to ND4, overall haplotype (Hd) and nucleotide

323   (Π) diversities were 0.930 ± 0.008 and 0.020 ± 0.0008, respectively. Across the

324   analysed mountain regions, Guadarrama Mountains showed lower ND4 genetic

325   diversity values (Hd = 0.290 ± 0.109, Π = 0.001 ± 0.0002) compared to the other

326   regions (eastern Pyrenees: Hd = 0.770 ± 0.039, Π = 0.002 ± 0.0003; central Pyrenees:

327   Hd = 0.724 ± 0.101, Π = 0.014 ± 0.003; central-western Pyrenees: Hd = 0.805 ± 0.027,

328   Π = 0.002 ± 0.0002; Picos de Europa: Hd = 0.602 ± 0.091, Π = 0.003 ± 0.001).

329   For microsatellite loci, we did not find evidence of large allele dropout,

330   stuttering or null allele artefacts. Similarly, no significant linkage disequilibrium or

331   departures from HWE across populations and loci were detected after applying the

332   Bonferroni correction. Observed (H_O) and expected heterozygosity (H_E) ranged from

333   0.197 to 0.794 and from 0.222 to 0.720, respectively (mean H_O = 0.473, mean H_E =

334   0.530; S1 Table). Mean number of alleles (Na) and allelic richness (Ar) varied from

335   2.059 to 7.824 and from 1.270 to 5.620, respectively (mean Na = 4.440, mean Ar =

336   1.873), and the inbreeding coefficient (F_{IS}) ranged from -0.110 to 0.403 (mean =

337   0.157). Among the analysed mountain regions, Picos de Europa and the eastern

338   Pyrenees were the richest regions in terms of genetic diversity, whereas Guadarrama

339   Mountains was the poorest, with the central and central-western Pyrenees

340   presenting intermediate values (Table 1). With regard to lowland areas, populations

341   located in the Duero and Ebro basins (herein referred to as Guadarrama lowland

342   localities) were the most diverse, while eastern Pyrenean localities were the least

343   diverse.

344

Phylogenetic analyses

346   From the 219 individuals analysed for the ND4 gene we identified 34

347   haplotypes, of which 22 are newly described (Fig 3, S1 Table). Haplotypes were

348   defined by 61 polymorphic sites, of which 49 were parsimony informative. The

349   majority of newly described haplotypes were found in the Pyrenees (13), whereas

350   only three and one haplotypes were detected in Picos de Europa and Guadarrama

351   Mountains, respectively; the remaining five haplotypes were found in lowland

352   localities. The haplotype network showed that haplotypes clustered into four well-

353   differentiated haplogroups with a strong association with geography (Figs 3 and S2a):

354   haplogroup A included sequences from Guadarrama and corresponding lowland

355   areas (corresponding to populations of *A. o. pertinax*), haplogroup F included

356   sequences from the eastern Pyrenees (corresponding to populations of *A.*

357   *almogavarii*), haplogroup E corresponded to populations from the central Pyrenees

358   (*A. a. inigoi*), and haplogroup B (corresponding to populations of *A. o. obstetricans*)

359   included sequences from the central-western Pyrenees and Picos de Europa. Within

360   haplogroup B, sequences corresponding to central-western Pyrenean populations

361   were clearly separated from those from Picos de Europa. In addition, in four localities

362   we detected the presence of more than one haplogroup (Figs 3 and S2a, S1 Table):

363   haplogroups A and B were found to co-occur in population Fte. Nueva de Bardales

364   (T2), whereas both haplogroups B and E were found in populations Plano de Igüer

365   (PI), Balsa Pertacua (BP) and Ibón de los Asnos (61XR).

366

367   **Fig 3. Haplotype network of ND4 sequences analysed in *Alytes***

368   ***obstetricans/almogavarii*.** Each circle represents a unique haplotype and the circle

369   area is proportional to the number of sequences of a given haplotype. Blue dots

370   correspond to inferred unsampled haplotypes. Sequences depicted in white were

371   retrieved from GenBank. The analysed high mountain regions and corresponding

372   lowland areas are indicated by different colours: eastern Pyrenees (EPY, orange),

373   central Pyrenees (CPY, grey), central-western Pyrenees (CWPY, pink), Picos de Europa

374   mountains (PEU, yellow), and Guadarrama Mountain Range and corresponding

375   lowland areas (GUA, blue).

376

377   In order to describe the affinities between the different haplogroups, we built

378   a consensus tree with the five sequenced gene fragments using a multispecies

379   coalescent approach (species tree; *BEAST). The tree placed lineage E at the base of

380   the *A. obstetricans/almogavarii* lineages, with lineage A as sister to lineage B. Finally,

381   lineage B split into central-western Pyrenees and Picos de Europa groups (S3 Fig).

382

Genetic structure and effective population sizes

384   All the clustering analyses performed on microsatellites recovered congruent

385   results (Figs 4, 5 and S2). Regarding DAPC analysis, the optimum number of clusters

386   was inferred to be 7 (Figs 4c, S2b and S4b). The inferred clusters were consistent with

387   the geographic location of populations. A closer look from K = 2 to K = 7 revealed a

388   spatial hierarchical genetic structure (S4a Fig), with a first split between the central-

389   western Pyrenees and all other populations, and a subsequent subdivision of this

390   second group into central Pyrenees–eastern Pyrenees and Guadarrama and

391   corresponding lowland populations–Picos de Europa. At K = 4, populations from the

392   Guadarrama Mountain Range split from lowland populations located in the Duero

393   and Ebro basins and Picos de Europa Mountains, whereas at K = 5 there was a split

394   between the central and eastern Pyrenees. The following splits occurred within the

395   central-western Pyrenean group. According with DAPC analysis, the PCA grouped

396   populations according to their geographic distribution rather than by described

19

397   subspecies (Fig 4d). PC1 separated the Pyrenees from the Picos de Europa and

398   Guadarrama, whereas PC2 distributed Pyrenean populations along the Pyrenean

399   chain and contributed to the separation of the Picos de Europa and Guadarrama.

400   STRUCTURE analysis showed patterns of genetic differentiation similar to those

401   inferred by PCA, and identified K = 2 as the best clustering solution (Figs 4a and S5):

402   the first cluster grouped together all Pyrenean populations and the second cluster

403   included peninsular ones. A smaller peak was detected at K = 7 (Fig 4a, 5 and S5b), in

404   agreement with DAPC-inferred clusters, but segregating populations located in the

405   Duero and Ebro basins from Guadarrama Mountains, while splitting central-western

406   Pyrenean populations into two groups. This partitioning into seven clusters was also

407   supported by results of Tess3R analyses (S6 Fig). Furthermore, a higher level of

408   genetic admixture was detected in lowland populations than in highland populations

409   (Figs 5 and S6). More into detail, lowland *A. o. pertinax* populations generally

410   presented the highest degree of admixture, whereas in the Pyrenees moderate levels

411   of admixture were detected between *A. almogavarii* lineage E and *A. obstetricans* in

412   the west, as well as between the two *A. obstetricans* lineages, but not between the

413   two *A. almogavarii* lineages (Fig 5). In order to describe the segregation history

414   amongst the seven groups identified by STRUCTURE, we built a NJ tree based on net

415   nucleotide distances: the tree started at K = 3 with the separation of Guadarrama and

416   corresponding lowland populations from Picos de Europa and the Pyrenees, then at K

417   = 4 populations from the central and eastern Pyrenees split from central-western

418   Pyrenean populations, whereas the following splits occurred within the different

419   major groups (Fig 4b). We also built a second NJ tree inferred from microsatellite-

420   based D_A distances over all populations that identified five discrete lineages, which

421   match with ND4-inferred lineages, except that populations included in haplogroup B

422   formed two separate groups (S2d and S7 Figs). Nevertheless, the tree suggested that

423   the pairs of lineages central Pyrenees–eastern Pyrenees and Guadarrama–Picos de

424   Europa were more closely related with each other than with the lineage of central-

425   western Pyrenees, which in turn appeared more distant from the rest of the lineages.

426

427   **Fig 4. Results of clustering analyses of *Alytes obstetricans/almogavarii* populations**

428   **based on microsatellite data.** (a) STRUCTURE barplots of membership assignment for K =

429   2 and K = 7. Each individual is represented by a vertical bar corresponding to the

430   assignment probabilities to the K cluster. White lines separate populations and black lines

431   separate clusters. (b) Neighbour-joining tree based on net nucleotide distances among

432   the seven clusters inferred by STRUCTURE. Arrows indicate the sequence of

433   differentiation when K increases. (c) Summary plot from Discriminant Analysis of Principal

434   Components (DAPC) for K = 7 genetic clusters. Dots represent individuals and genetic

435   clusters are shown as inertia ellipses. (d) Plot obtained in the Principal Component

436   Analysis (PCA). Each dot represents one individual. Labels indicate the different genetic

437   clusters: eastern Pyrenees (EPY, orange), central Pyrenees (CPY, grey), central-western

438   Pyrenees (CWPY, pink), Picos de Europa mountains (PEU, yellow), and Guadarrama

439   Mountain Range (GUA, blue).

440

441   **Fig 5. Results of Bayesian clustering analysis (STRUCTURE) for K = 7 microsatellite**

442   **groups for *Alytes obstetricans/almogavarii*.** Sampled populations are represented by

443   pie charts highlighting the population cluster membership obtained in STRUCTURE.

444   The inset map shows the distribution of the main lineages: orange - ND4 haplogroups

445   E-F (*A. almogavarii*), yellow - ND4 haplogroup B (*A. o. obstetricans*), blue - ND4

446   haplogroup A (*A. o. pertinax*), red - ND4 haplogroup C (*A. o. boscai*), green - ND4

447   haplogroup D (*A. o. boscai*), black - unclear (adapted from Dufresnes and Martínez-

448   Solano [23]).

449

450

451   The test of significance of pairwise F_{ST} values between the seven lineages

452   defined by STRUCTURE was significantly different from zero (P < 0.01; S3 Table),

453   indicating significant genetic differences. ND4-based pairwise F_{ST} values ranged from

454   0.951 for eastern Pyrenees–Guadarrama Mountains to 0.089 for Guadarrama

455   Mountains–Guadarrama lowlands, whereas microsatellite-based pairwise F_{ST} values

456   ranged from 0.222 for Guadarrama Mountains–central-western Pyrenees to 0.060 for

457   Guadarrama lowlands–Picos de Europa. Accordingly, AMOVA analyses suggested

458   significant structure among the seven genetic lineages (P < 0.001; S4 Table). The

459   proportion of variation attributable to differences among lineages was lower in

460   microsatellites (26.171%) than in ND4 (84.945%), possibly as a result of gene flow and

461   the inability of mtDNA to detect it. Conversely, variation among individuals within

462   populations was low for ND4 (8.736%) and high for microsatellite (56.425%) markers,

463   as expected for polymorphic loci such as microsatellites.

464   In the Pyrenees, microsatellite genetic differentiation followed a ring-like

465   pattern, being maximal between lineages EPY (orange) and CWPY (pink; at opposite

466   extremities on PCA axis 2, Fig 4c-d), even though they are geographically proximate in

467   the central and eastern Pyrenees. To evaluate this hypothesis of ring-shaped isolation

468   by distance, we correlated genetic distances (F_{ST} obtained from microsatellites) of

469   Pyrenean populations to different types of geographic distance. We obtained a weak

470   isolation by distance pattern between genetic differentiation and Euclidean

471   geographic distance (Mantel's R = 0.185, P = 0.002; Fig 6). In contrast, we detected a

472   strong correlation between genetic differentiation and the geographic distance

473   suggested by PCA analysis (Fig 4c-d), which assumed no direct gene flow across the

474   central Pyrenean axis and thus between the two most genetically differentiated

475   lineages EPY and CWPY (Mantel's R = 0.683, P = 0.001; Fig 6).

476

477   **Fig 6. Isolation by distance analysis over *Alytes obstetricans/almogavarii***

478   **population pairs from the Pyrenees.** Isolation by distance was calculated based on

479   (a) Euclidean geographic distance between all pairs of populations (Mantel's R =

480   0.185, P = 0.002) and (b) corrected geographic distance as suggested by PCA analysis,

481   i.e. following a ring-shaped distribution around the Pyrenean chain (Fig 4; Mantel's R

482   = 0.683, P = 0.001).

483

484

485   The estimation of effective population sizes conducted in Colony returned, in

486   general, low values (S1 Table). Values ranged from five in the population Laguna de

487   Pájaros (LP) to 160 breeding individuals in the population Lago Ercina (ERC), with a

488   mean N_e of 43. The lowest values were found in populations from the Guadarrama

489   Mountains (N_e range = 5–15), while higher values were found in the Pyrenees

490   (eastern Pyrenees: 14–51, central Pyrenees: 68, central-western Pyrenees: 12–84)

491   and Picos de Europa (19–160).

492

493   **Demographic history**

494   DIYABC analyses suggested highest support for two different but compatible

495   scenarios of population divergence depending on the genetic markers used (i.e.

496   scenario 2 when using only microsatellites and scenario 5 when combining

497   microsatellites and ND4; Fig 2b, S5 Table). Both scenarios had non-overlapping 95%

498   confidence intervals and type I and II errors for the best supported models were low

499   (S5 Table), indicating high confidence in scenario choice. Model checking confirmed

500   that the best supported scenarios provided a good fit to the observed data (data not

501   shown). Furthermore, the mean mutation rate estimated for ND4 was found to be an

502   order of magnitude higher than the literature value (1.96×10^{-7}

503   substitutions/site/year; S6 Table), but still much lower than that estimated for

504   microsatellites (ranging from 1.28×10^{-4} to 3.89×10^{-4} and from 4.59×10^{-5} to $3.31 \times$

505   10^{-4} for analyses conducted using only microsatellites and including both ND4 and

506   microsatellite markers, respectively).

507   The analysis focused on microsatellites indicated that scenario 2 (the

508   sequential splitting model based on results from clustering analyses) was the best

509   supported model (Fig 2b, S5 Table). According to this scenario, the first split led to

510   the separation of Pyrenean populations from peninsular ones. During the second split

511   there was the divergence of, on the one hand, central-western and central-eastern

512   Pyrenean populations, and on the other Picos de Europa and Guadarrama

513   populations. Finally, populations from the central Pyrenees originated from eastern

514   Pyrenean populations during the third split. The first split occurred 56 000–28 000

515   years ago, and the second and third splits 36 800–18 400 and 25 200–12 600 years

516   ago, respectively (S6 Table). The analysis based on the combination of microsatellites

517   and ND4, however, suggested that Picos de Europa populations were generated by

518   admixture of populations from the central-western Pyrenees and Guadarrama

519   (scenario 5; Fig 2b, S5 Table). Results indicated that the first split occurred 76 200–38

520   100 years ago, the second split 52 800–26 400 years ago and the admixture event 41

521   400–20 700 years ago (S6 Table).

25

522

Discussion

523

524   The Iberian Peninsula is an extraordinary model system to assess the multiple

525 historical vicariance events of species, the so called "refugia within refugia" model,

526 where mountain ranges have had a significant role [11, 12]. Such processes are

527 influenced by climatic and topographic conditions as well as through biological

528 processes between populations, which in turn reflect different and contrasting time

529 scales, historical and contemporary. To unravel such complex scenarios, a multilocus

530 approach is expected to reveal contrasting, often discordant findings that underline

531 intricate evolutionary processes [57]. Several recent studies targeting the Iberian

532 Peninsula and the Mediterranean biodiversity hotspot have focused on the processes

533 of niche divergence and admixture following secondary contact (e.g. Chamorro et al.

534 [58] and Martínez-Freiría et al. [59] with Mediterranean vipers, Antunes et al. [60]

535 with the fire salamander *Salamandra salamandra*, and Dufresnes et al. [61] with

536 *Discoglossus* and *Pelodites* frogs), highlighting the role of these areas as centres of

537 diversification and speciation. The results of the present study revealed a strong

538 association of the defined genetic lineages with geography by using a multilocus

539 analysis of genetic divergence in Iberian high mountain populations of *A.*

540 *obstetricans*/*almogavarii*. Furthermore, high mountain populations showed higher

541 levels of genetic distinctiveness than lowland populations (Fig 5), suggesting that

542   mountains may have driven population differentiation through long-term geographic

543   isolation, with lowlands more likely to be dispersal corridors for *A.*

544   *obstetricans/almogavarii,* as it has been described for other species (see e.g. [62,

545   63]).

546

The role of high mountains in genetic differentiation and glacial refugia

549   This study describes the presence of seven different nuclear microsatellite

550   clusters, that are likely a result of recent microrefugial areas within the Pyrenees (Fig

551   5). Most of the recovered genetic structure was within Pyrenean populations, which

552   in turn were genetically more related to each other than with the other two high

553   mountain areas. Putative episodes of admixture within *A. obstetricans/almogavarii* in

554   the Pyrenees were suggested by previous phylogenetic analyses [3]. Following the

555   splits between major population lineages in *A. obstetricans/almogavarii*, which date

556   back to the Early Pleistocene (starting from 2.5 Mya; [20]), there have been several

557   glacial-interglacial episodes that likely provided opportunities for diverging taxa to

558   come into contact and interbreed following range shifts tracking the climatic

559   fluctuations [12, 64]. Our findings show that Pyrenean high mountain populations

560   have gone through relatively recent events of admixture, likely favoured by the

561   different glacial-interglacial episodes that characterised the Late Pleistocene.

562   Specifically, according to ABC analyses, the two lineages ascribed to *A. almogavarii*

563   (E-F, central and eastern Pyrenees), together with some populations of *A. o.*

564   *obstetricans* (central-western Pyrenean group) seem to have undergone a certain

565   degree of contact and admixture until divergence took place ~36 800–12 600 years

566   ago (Fig 2b). Despite the selected model, which proposes two independent admixture

567   events between the three lineages, the highly overlapping dates together with the

568   significant ring-shaped isolation by distance pattern (Fig 6; see below) suggest that

569   one single admixture event might have occurred within one main glacial refugia

570   where the three lineages coincided. In addition, contemporary signs of connectivity

571   between the two species were detected at lineage borders, as indicated by the

572   occurrence of a contact zone between ND4 lineage E and *A. o. obstetricans* in the

573   west (Figs 3, 5 and S2). Similarly, signs of admixture and extensive gene flow between

574   *A. o. obstetricans* and *A. almogavarii* in the western Pyrenees were previously

575   pointed out by allozyme markers [25, 26]. In contrast, in the central and eastern

576   Pyrenees no signs of connectivity were detected between ND4 lineage F and either

577   lineage E or *A. o. obstetricans*. This scenario of different contact zones telling

578   different stories is exemplified in ring species, i.e. a system formed by a region of

579   interconnected populations with both ends of the ring coming into contact without

580   apparent admixture [65, 66]. In the Pyrenees, the spatial distribution of the *A.*

581   *obstetricans* complex seems to fit with a postglacial colonisation pattern similar to

582   what has been described in ring diversification, where taxa at the western part of the

28

583 ring likely interbreed and those at the eastern side apparently don't, displaying a

584 continuum from slightly divergent neighbouring populations to substantially

585 reproductively isolated taxa (Figs 4d, 5 and 6). Ring diversifications represent cases of

586 population divergence around a geographical barrier in a ring-like manner [67] that

587 can result in cases of speciation in action (i.e. ring species) and have been cited as

588 evidence of evolution [68], with some of the most well-known cases being identified

589 in herptiles, such as the *Ensatina eschscholtzii* salamander complex [69] and the

590 western fence lizard *Sceloporus occidentalis* [70] in western North America. In light of

591 this, our results are not entirely in line with the distinction of *A. almogavarii* as a

592 different species, yet support a scenario of speciation in action, with lineage F

593 showing evidence for speciation and reproductive isolation [23], and lineage E

594 retaining some degree of connectivity with *A. o. obstetricans*. Nevertheless, we

595 cannot rule out that this pattern may be the result of geographic sampling gaps, and

596 additional surveys across hybrid zones between lineages E-F and *A. o. obstetricans*, as

597 well as further work using resistance distances (i.e. by taking elevation, slope and

598 land cover into account), would be required to fully test the ring species hypothesis.

599 Finally, with regard to the central-western Pyrenean group, the subdivision by

600 microsatellite analyses into two or three different genetic clusters (Figs 4 and S2),

601 points to a scenario of allopatric divergence after the recolonization of the Pyrenees

602 as a result of geographic barriers, with consequent reduction or disruption of gene

603 flow. Alternatively, this differentiation might have happened during one of the abrupt

604 cooling episodes of the Holocene (e.g. the 8 200 year-event; [71]), with consequent

605 isolation in separate glacial refugia. Range isolation and lineage divergence in

606 separate Pyrenean refugia during Pleistocene glacial cycles were also invoked e.g. for

607 the Pyrenean brook newt *Calotriton asper* [55], the ground-dwelling spider

608 *Harpactocrates ravastellus* [72], the rusty-leaved alpenrose *Rhododendron*

609 *ferrugineum* [73] and the snapdragon *Antirrhinum* [74], in line with evidence from a

610 number of other high mountain areas that served as glacial refugia during periods of

611 adverse conditions, such as the Andes, Himalaya and the Southern Alps in New

612 Zealand (see [64] for a review). From a conservation point of view, we suggest that

613 these areas should be treated as separate conservation and management units.

614

Mito-nuclear discordances

616 The analyses of microsatellites distinguished two highly divergent *A. o.*

617 *obstetricans* lineages, one in the central-western Pyrenees and the other in Picos de

618 Europa (Figs 4 and S2), with the latter being more genetically related to the southern

619 populations (ascribed to *A. o. pertinax*; Figs 4d and S7). In contrast, these two

620 lineages bear the same mtDNA (ND4) haplogroup ascribed to *A. o. obstetricans*

621 (haplogroup B; Figs 3 and S2a). One possible explanation is that the closer genetic

622 affinity of the western and southern area populations rather than to the central-

623 western Pyrenean lineage originated from extensive admixture with *A. o.*

624   *obstetricans* (the central-western Pyrenean group) as the maternal donor and *A. o.*

625   *pertinax* as the paternal donor (Fig 2b). A similar pattern was observed in *S.*

626   *salamandra* [75] and in crustaceans of the genus *Daphnia* [76]. A plausible scenario

627   could be that, during Late Pleistocene glacial periods (as suggested by results from

628   DYABC modelling when combining both microsatellites and mtDNA; Fig 2), some *A. o.*

629   *obstetricans* populations remained confined in isolated refugia where they coincided

630   with *A. o. pertinax* for a sufficient time so that genetic admixture could take place.

631   Similarly, range isolation during Pleistocene climatic fluctuations was suggested for

632   the cryptic *Pelodytes* anuran clade [77, 78], the Cabrera vole *Microtus cabrerae* [79]

633   and the scrub-legume grasshopper *Chorthippus binotatus binotatus* [80], where

634   extant lineages likely diverged in separated refugia within the Iberian Peninsula.

635   Subdivided glacial refugia could have experienced events of admixture during the

636   succession of glacial and interglacial periods, with consequent fusion between

637   refugial lineages [81, 82].

638   Mito-nuclear discordances with evidence for admixture or hybridisation are

639   not uncommon in amphibians (e.g. [4, 8, 60]) and have also been described in a wide

640   range of other animal species from north-central Iberian Peninsula, from arachnids

641   [83] to mammals [84]. Furthermore, the Cantabrian Mountains represent a peculiar

642   biogeographic region and a recognised hotspot of genetic diversity in amphibians,

643   being home to endemic refugial clades in a number of species with broad European

644   distribution [82, 85]. Finally, more recently, the Picos de Europa and *A. o. pertinax*

31

645   populations may have come into secondary contact and interbred following an

646   expansion phase, creating zones of admixture at lineage borders. Alternatively, the

647   discordance may stem from stochastic processes in the form of genetic drift, and the

648   phylogeographic structure detected in mtDNA (Figs 3 and S3) may have developed as

649   a result of low individual dispersal distances and/or population sizes [86], as

650   evidenced by our results and published literature (e.g. [87]). Further studies and

651   sequencing of more molecular markers are needed to test these hypotheses and

652   enrich our understanding of the phylogeography of *A. obstetricans*.

653

Chytridiomycosis and population bottleneck

655   The genetic distinctiveness and limited genetic diversity of populations from

656   the Guadarrama Mountains herein detected (Figs 4 and S2, Table 1) are likely early

657   signs of inbreeding depression induced by an emerging pathogen, i.e. the chytrid

658   fungus *Batrachochytrium dendrobatidis* [88]. It should be noted that our sampling

659   was performed approximately 10 years after an epidemic of the disease

660   chytridiomycosis, which hugely impacted this area in the period 1997–1999, causing

661   several populations to decrease or even disappear [16, 89]. Accordingly, the only

662   sampled population in the affected area that did not show signs of chytridiomycosis

663   was the one presenting the highest genetic diversity (Montes de Valsain, MV; S1

664   Table). Our findings complement those of Albert et al. [18] that detected evidence of

665   low genetic variability and strong population bottleneck in *A. obstetricans* from the

666   same mountain system. In addition to this, we report on the first estimates of

667   effective population sizes of these populations, which were among the lowest overall

668   (N_e = 5–15; Table 1), raising concern for the long-term persistence of these

669   populations, which are small and isolated. Indeed, the closest neighbouring

670   populations are located more than 50 km away and are known to be small and not

671   genetically related [18, 90]. Furthermore, the Guadarrama Mountains constitute a

672   major barrier to gene flow in amphibians and a key feature shaping population

673   structure and promoting population divergence across taxa [62]. Our results are an

674   example of a disease acting as selective pressure in wild populations by inducing

675   genetic hallmarks of bottlenecks and inbreeding, as it has also been shown in other

676   species such as the black-tailed prairie dog (*Cynomys ludovicianus*), the mountain

677   yellow-legged frog (*Rana muscosa*) and the bobcat (*Lynx rufus*) (reviewed in [91]).

678

679   ## Differences in the evolutionary horizon/resolution between

680   ## genetic markers

681   This study confirms previous findings in *A. obstetricans/almogavarii* clades

682   [20] with the only difference that our species tree analyses recovered a different

683   basal lineage (S3 Fig), a likely consequence of our limited inference power given that

684   only two loci were used for species tree reconstruction. Results from ABC modelling

685   based on either microsatellites or microsatellites + mtDNA resulted in time estimates

686   highly different from those of the species tree (Fig 2b), suggesting that the two

687   analyses are depicting different evolutionary events. In fact, while the species tree

688   has proven useful to estimate divergence times associated with the formation of

689   species/subspecies, ABC modelling was here employed to gain insights into the

690   colonisation of three high mountain regions in the Iberian Peninsula by the different

691   *A. obstetricans/almogavarii* taxa. Microsatellite markers, with their faster mutation

692   rate, are known to perform poorly for the estimation of ancient historical events [57,

693   92]. On the contrary, microsatellites provide substantially better estimations than

694   mtDNA for the most recent dynamics [57]. However, the combination of both

695   markers in our ABC modelling resulted in similar divergence times as those estimated

696   using microsatellites alone. It is thus possible that combining both markers may have

697   biased toward microsatellites and the estimation of recent historical events.

698   We need to stress that DIYABC modelling has some uncertainty. Firstly, this

699   approach is based on scenarios where no gene flow is permitted between

700   populations after they initially diverge. Only single events of admixture between

701   populations are considered, whereas recurrent gene flow due to dispersal cannot be

702   incorporated. However, population structure analyses were used to investigate

703   contemporary gene flow and identify patterns of admixture and contact zones at

704   lineage borders (e.g. Fig 5). Secondly, the tested models do not represent a

705   comprehensive range of all possible scenarios, but are instead based on a selection of

706   contrasting hypotheses that we considered were most likely to reflect our data. We

707   focused our analysis on simple contrasting models aimed at capturing the key

708   demographic events, avoiding overcomplex and redundant models, therefore the

709   selected models should be viewed as a starting point for evolutionary understanding.

710   This approach has proven useful to increase the ability of DIYABC to reveal the

711   correct model, as well as to better estimate the error and accuracy of parameter

712   estimates [93]. On the other hand, it has to be noted that estimates based on

713   mitochondrial data might be unreliable due to the erratic mutation rate of mtDNA

714   and to the fact that mtDNA does not evolve neutrally since transmission of

715   mitochondria is completely linked to maternal inheritance. Indeed, mtDNA-based

716   estimates have been found to mismatch the onset of species divergence in both

717   directions due to the stochasticity of coalescence [94].

718

Concluding remarks

720   Our multilocus phylogeography across the Iberian Peninsula revealed high

721   genetic structure correlated with geography and a complex pattern of lineage

722   admixture in high mountain populations of *A. obstetricans*/*almogavarii*. Our study

723   evidenced how each analysed mountain region underwent a peculiar

724   phylogeographic history through the Late Pleistocene, which is consistent with the

725   "refugia within refugia" model [11, 12] and confirms previous studies on a number of

726   Iberian amphibian species (e.g. [22, 77, 85, 95, 96]). Results also support the

727   assumption that refugia within refugia may be hotspots of extensive mito-nuclear

35

728   discordances [82], highlighting the importance of multilocus approaches to infer the

729   dynamics of population divergence. Environmental change in the different mountain

730   systems may have an influence on selection, resulting in an increased divergence

731   among isolated populations, consequently leading to speciation [97]. The phenetic

732   differences between the subspecies of *Alytes* (especially *A. o. pertinax*) may be a

733   further indication of adaptation to some micro-environmental differences such as

734   streams vs still waters (known to influence coloration in *Alytes*, [98]), temperature

735   and solar radiation at different altitudes between the studied mountain systems.

736

Acknowledgements

References

1. Avise JC. Phylogeography: The history and formation of species. (ELS) iEoLS, editor. Cambridge, MA, USA: Harvard University Press; 2000.

2. Fordham DA, Brook BW, Moritz C, Nogués-Bravo D. Better forecasts of range dynamics using genetic data. Trends in Ecology & Evolution. 2014;29(8):436-43.

3. Gonçalves H, Martínez-Solano I, Ferrand N, García-París M. Conflicting phylogenetic signal of nuclear vs mitochondrial DNA markers in midwife toads (Anura, Discoglossidae, *Alytes*): Deep coalescence or ancestral hybridization? Molecular Phylogenetics and Evolution. 2007;44(1):494-500.

4. Pereira RJ, Martinez-Solano I, Buckley D. Hybridization during altitudinal range shifts: Nuclear introgression leads to extensive cyto-nuclear discordance in the fire salamander. Molecular Ecology. 2016;25(7):1551-65.

5. Denton RD, Kenyon LJ, Greenwald KR, Gibbs HL. Evolutionary basis of mitonuclear discordance between sister species of mole salamanders (*Ambystoma* sp.). Molecular Ecology. 2014;23(11):2811-24.

6. Edwards SV, Potter S, Schmitt CJ, Bragg JG, Moritz C. Reticulation, divergence, and the phylogeography–phylogenetics continuum. Proceedings of the National Academy of Sciences. 2016;113(29):8025-32.

7. Toews DPL, Brelsford A. The biogeography of mitochondrial and nuclear discordance in animals. Molecular Ecology. 2012;21(16):3907-30.

8. Bisconti R, Porretta D, Arduino P, Nascetti G, Canestrelli D. Hybridization and extensive mitochondrial introgression among fire salamanders in peninsular Italy. Scientific Reports. 2018;8(1):1-10.

9. Hewitt GM. The genetic legacy of the Quaternary ice ages. Nature. 2000;405(6789):907-13.

10. Hewitt GM. Genetic consequences of climatic oscillations in the Quaternary. Philosophical Transactions of the Royal Society of London B: Biological Sciences. 2004;359(1442):183-95; discussion 95.

11. Gómez A, Lunt DH. Refugia within refugia: Patterns of phylogeographic concordance in the Iberian Peninsula. In: Weiss S, Ferrand N, editors. Phylogeography of southern European refugia. Amsterdam, Netherlands: Springer; 2007. p. 155-88.

12. Abellán P, Svenning J-C. Refugia within refugia–patterns in endemism and genetic divergence are linked to Late Quaternary climate stability in the Iberian Peninsula. Biological Journal of the Linnean Society. 2014;113(1):13-28.

13. Hewitt GM. Some genetic consequences of ice ages, and their role in divergence and speciation. Biological Journal of the Linnean Society. 1996;58(3):247-76.

14. Bosch J, Beebee T, Schmidt B, Tejedo M, Martinez Solano I, Salvador A, et al. *Alytes obstetricans* (errata version published in 2016). The IUCN Red List of Threatened Species 2009: e.T55268A87541047. doi:10.2305/IUCN.UK.2009.RLTS.T55268A11283700.en. 2009.

15. Miró A, Sabás I, Ventura M. Large negative effect of non-native trout and minnows on Pyrenean lake amphibians. Biological Conservation. 2018;218:144-53.

784   16.   Bosch J, Martínez-Solano I, García-París M. Evidence of a chytrid fungus infection
785   involved in the decline of the common midwife toad (*Alytes obstetricans*) in
786   protected areas of central Spain. Biological Conservation. 2001;97(3):331-7.
787   17.   Tobler U, Schmidt BR. Within- and among-population variation in chytridiomycosis-
788   induced mortality in the toad *Alytes obstetricans*. PLoS One. 2010;5(6):e10927.
789   18.   Albert EM, Fernández-Beaskoetxea S, Godoy JA, Tobler U, Schmidt BR, Bosch J.
790   Genetic management of an amphibian population after a chytridiomycosis outbreak.
791   Conservation Genetics. 2014;16(1):103-11.
792   19.   Walker SF, Bosch J, Gomez V, Garner TW, Cunningham AA, Schmeller DS, et al.
793   Factors driving pathogenicity vs. prevalence of amphibian panzootic chytridiomycosis
794   in Iberia. Ecology Letters. 2010;13(3):372-82.
795   20.   Gonçalves H, Maia-Carvalho B, Sousa-Neves T, Garcia-Paris M, Sequeira F, Ferrand N,
796   et al. Multilocus phylogeography of the common midwife toad, *Alytes obstetricans*
797   (Anura, Alytidae): Contrasting patterns of lineage diversification and genetic
798   structure in the Iberian refugium. Molecular Phylogenetics and Evolution.
799   2015;93:363-79.
800   21.   Maia-Carvalho B, Gonçalves H, Martínez-Solano I, Gutiérrez-Rodríguez J, Lopes S,
801   Ferrand N, et al. Intraspecific genetic variation in the common midwife toad (*Alytes*
802   *obstetricans*): Subspecies assignment using mitochondrial and microsatellite markers.
803   Journal of Zoological Systematics and Evolutionary Research. 2014;52(2):170-5.
804   22.   Maia-Carvalho B, Vale CG, Sequeira F, Ferrand N, Martínez-Solano I, Gonçalves H. The
805   roles of allopatric fragmentation and niche divergence in intraspecific lineage
806   diversification in the common midwife toad (*Alytes obstetricans*). Journal of
807   Biogeography. 2018;45(9):2146-58.
808   23.   Dufresnes C, Martínez-Solano Í. Hybrid zone genomics supports candidate species in
809   Iberian *Alytes obstetricans*. Amphibia-Reptilia. 2019;41(1):105-12.
810   24.   Dufresnes C, Hernandez A. Phylogeographic advances in midwife toads (*Alytes*)
811   support the existence of a novel taxon endemic to the Central Pyrenees. Journal of
812   Zoological Systematics Evolutionary Research. 2021;59(8):2170-9.
813   25.   Arntzen JW, Garcia-Paris M. Morphological and allozyme studies of midwife toads
814   (genus *Alytes*), including the description of two new taxa from Spain. Contributions
815   to Zoology. 1995;65(1):5-34.
816   26.   García-París M. Variabilidad genética y distribución geográfica de *Alytes obstetricans*
817   *almogavarii* en España. Revista Española de Herpetología. 1995;9:133-8.
818   27.   Pöschel J, Heltai B, Graciá E, Quintana MF, Velo-Antón G, Arribas O, et al. Complex
819   hybridization patterns in European pond turtles (*Emys orbicularis*) in the Pyrenean
820   Region. Scientific Reports. 2018;8(1):1-13.
821   28.   Montero-Pau J, Gómez A, Muñoz J. Application of an inexpensive and high-
822   throughput genomic DNA extraction method for the molecular ecology of
823   zooplanktonic diapausing eggs. Limnology and Oceanography: Methods.
824   2008;6(6):218-22.
825   29.   Kumar S, Stecher G, Tamura K. MEGA7: Molecular Evolutionary Genetics Analysis
826   version 7.0 for bigger datasets. Molecular Biology and Evolution. 2016;33(7):1870-4.
827   30.   Flot JF. SeqPHASE: a web tool for interconverting PHASE input/output files and FASTA
828   sequence alignments. Molecular Ecology Resources. 2010;10(1):162-6.

829   31.   Stephens M, Donnelly P. A comparison of bayesian methods for haplotype
830   reconstruction from population genotype data. The American Journal of Human
831   Genetics. 2003;73(5):1162-9.
832   32.   Stephens M, Smith NJ, Donnelly P. A new statistical method for haplotype
833   reconstruction from population data. The American Journal of Human Genetics.
834   2001;68(4):978-89.
835   33.   Kearse M, Moir R, Wilson A, Stones-Havas S, Cheung M, Sturrock S, et al. Geneious
836   Basic: An integrated and extendable desktop software platform for the organization
837   and analysis of sequence data. Bioinformatics. 2012;28(12):1647-9.
838   34.   Van Oosterhout C, Hutchinson WF, Wills DPM, Shipley P. MICRO-CHECKER: Software
839   for identifying and correcting genotyping errors in microsatellite data. Molecular
840   Ecology Notes. 2004;4(3):535-8.
841   35.   Rousset F. GENEPOP'007: a complete re-implementation of the GENEPOP software
842   for Windows and Linux. Molecular Ecology Resources. 2008;8(1):103-6.
843   36.   Rice WR. Analyzing tables of statistical tests. Evolution. 1989;43(1):223-5.
844   37.   Peakall R, Smouse P. GenAlEx 6.5: Genetic analysis in Excel. Population genetic
845   software for teaching and research-an update. Bioinformatics. 2012;28(19):2537-9.
846   38.   Kalinowski ST. hp-rare 1.0: a computer program for performing rarefaction on
847   measures of allelic richness. Molecular Ecology Notes. 2005;5(1):187-9.
848   39.   Belkhir K, Borsa P, Chikhi L, Raufaste N, Bonhomme F. GENETIX 4.05, logiciel sous
849   Windows TM pour la génétique des populations. Laboratoire Génome, Populations,
850   Interactions, CNRS UMR 5000, Université de Montpellier II, Montpellier (France).
851   1996-2004.
852   40.   Salzburger W, Ewing GB, Von Haeseler A. The performance of phylogenetic
853   algorithms in estimating haplotype genealogies with migration. Molecular Ecology.
854   2011;20(9):1952-63.
855   41.   Darriba D, Taboada GL, Doallo R, Posada D. jModelTest 2: More models, new
856   heuristics and parallel computing. Nature Methods. 2012;9(8):772.
857   42.   Stamatakis A. RAxML-VI-HPC: maximum likelihood-based phylogenetic analyses with
858   thousands of taxa and mixed models. Bioinformatics. 2006;22(21):2688-90.
859   43.   Rozas J, Ferrer-Mata A, Sánchez-DelBarrio JC, Guirao-Rico S, Librado P, Ramos-Onsins
860   SE, et al. DnaSP 6: DNA sequence polymorphism analysis of large data sets. Molecular
861   Biology and Evolution. 2017;34(12):3299-302.
862   44.   Heled J, Drummond AJ. Bayesian inference of species trees from multilocus data.
863   Molecular Biology and Evolution. 2009;27(3):570-80.
864   45.   Drummond AJ, Rambaut A. BEAST: Bayesian evolutionary analysis by sampling trees.
865   BMC Evolutionary Biology. 2007;7(1):1-8.
866   46.   Jombart T, Devillard S, Balloux F. Discriminant analysis of principal components: A
867   new method for the analysis of genetically structured populations. BMC Genetics.
868   2010;11(1):94.
869   47.   R Core Team. R: A language and environment for statistical computing. Vienna,
870   Austria: R Foundation for Statistical Computing. http://www.R-project.org/. 2018.
871   48.   Pritchard JK, Stephens M, Donnelly P. Inference of population structure using
872   multilocus genotype data. Genetics. 2000;155(2):945-59.

873   49.   Takezaki N, Nei M, Tamura K. POPTREEW: web version of POPTREE for constructing
874   population trees from allele frequency data and computing some other quantities.
875   Molecular Biology and Evolution. 2014;31(6):1622-4.
876   50.   Caye K, Jay F, Michel O, François O. Fast inference of individual admixture
877   coefficients using geographic data. The Annals of Applied Statistics. 2018;12(1):586-
878   608.
879   51.   Excoffier L, Lischer HE. Arlequin suite ver 3.5: a new series of programs to perform
880   population genetics analyses under Linux and Windows. Molecular Ecology
881   Resources. 2010;10(3):564-7.
882   52.   Excoffier L, Smouse PE, Quattro JM. Analysis of molecular variance inferred from
883   metric distances among DNA haplotypes: Application to human mitochondrial DNA
884   restriction data. Genetics. 1992;131(2):479-91.
885   53.   Dufresnes C, Litvinchuk SN, Leuenberger J, Ghali K, Zinenko O, Stöck M, et al.
886   Evolutionary melting pots: a biodiversity hotspot shaped by ring diversifications
887   around the Black Sea in the Eastern tree frog (*Hyla orientalis*). Molecular Ecology.
888   2016;25(17):4285-300.
889   54.   Jones OR, Wang J. COLONY: A program for parentage and sibship inference from
890   multilocus genotype data. Molecular Ecology Resources. 2010;10(3):551-5.
891   55.   Lucati F, Poignet M, Miró A, Trochet A, Aubret F, Barthe L, et al. Multiple glacial
892   refugia and contemporary dispersal shape the genetic structure of an endemic
893   amphibian from the Pyrenees. Molecular Ecology. 2020;29(15):2904-21.
894   56.   Cornuet JM, Pudlo P, Veyssier J, Dehne-Garcia A, Gautier M, Leblois R, et al. DIYABC
895   v2.0: A software to make approximate Bayesian computation inferences about
896   population history using single nucleotide polymorphism, DNA sequence and
897   microsatellite data. Bioinformatics. 2014;30(8):1187-9.
898   57.   Emerson BC, Hewitt GM. Phylogeography. Current Biology. 2005;15(10):R367-R71.
899   58.   Chamorro D, Martínez-Freiría F, Real R, Muñoz AR. Understanding parapatry: How do
900   environment and competitive interactions shape Iberian vipers' distributions?
901   Journal of Biogeography. 2020.
902   59.   Martínez-Freiría F, Freitas I, Zuffi MA, Golay P, Ursenbacher S, Velo-Antón G. Climatic
903   refugia boosted allopatric diversification in western Mediterranean vipers. Journal of
904   Biogeography. 2020;47(8):1698-713.
905   60.   Antunes B, Velo-Antón G, Buckley D, Pereira R, Martínez-Solano I. Physical and
906   ecological isolation contribute to maintain genetic differentiation between fire
907   salamander subspecies. Heredity. 2021:1-14.
908   61.   Dufresnes C, Pribille M, Alard B, Gonçalves H, Amat F, Crochet P-A, et al. Integrating
909   hybrid zone analyses in species delimitation: Lessons from two anuran radiations of
910   the Western Mediterranean. Heredity. 2020;124(3):423-38.
911   62.   Sánchez-Montes G, Wang J, Ariño AH, Martínez-Solano Í. Mountains as barriers to
912   gene flow in amphibians: Quantifying the differential effect of a major mountain
913   ridge on the genetic structure of four sympatric species with different life history
914   traits. Journal of Biogeography. 2018;45(2):318-31.
915   63.   Li Y, Zhang X, Fang Y. Landscape features and climatic forces shape the genetic
916   structure and evolutionary history of an oak species (*Quercus chenii*) in East China.
917   Frontiers in Plant Science. 2019;10:1060.

918 64. Wallis GP, Waters JM, Upton P, Craw D. Transverse alpine speciation driven by
919   glaciation. Trends in Ecology & Evolution. 2016;31(12):916-26.
920 65. Alcaide M, Scordato ES, Price TD, Irwin DE. Genomic divergence in a ring species
921   complex. Nature. 2014;511(7507):83-5.
922 66. Irwin D, Wake D. Ring species. In: Kliman RM, editor. Encyclopedia of evolutionary
923   biology. 3. Oxford: Academic Press; 2016. p. 467–75.
924 67. Monahan WB, Pereira RJ, Wake DB. Ring distributions leading to species formation: a
925   global topographic analysis of geographic barriers associated with ring species. BMC
926   Biology. 2012;10(1):1-15.
927 68. Irwin DE, Irwin JH, Price TD. Ring species as bridges between microevolution and
928   speciation. Genetica. 2001;112-113:223-43.
929 69. Kuchta SR, Wake DB. Wherefore and whither the ring species? 2016;104(1):189-201.
930 70. Bouzid NM, Archie JW, Anderson RA, Grummer JA, Leaché AD. Evidence for
931   ephemeral ring species formation during the diversification history of western fence
932   lizards (*Sceloporus occidentalis*). Molecular Ecology. 2021.
933 71. Alley RB, Mayewski PA, Sowers T, Stuiver M, Taylor KC, Clark PU. Holocene climatic
934   instability: A prominent, widespread event 8200 yr ago. Geology. 1997;25(6):483-6.
935 72. Bidegaray-Batista L, Sánchez-Gracia A, Santulli G, Maiorano L, Guisan A, Vogler AP, et
936   al. Imprints of multiple glacial refugia in the Pyrenees revealed by phylogeography
937   and palaeodistribution modelling of an endemic spider. Molecular Ecology.
938   2016;25(9):2046-64.
939 73. Charrier O, Dupont P, Pornon A, Escaravage N. Microsatellite marker analysis reveals
940   the complex phylogeographic history of *Rhododendron ferrugineum* (Ericaceae) in
941   the Pyrenees. PLoS One. 2014;9(3):e92976.
942 74. Liberal IM, Burrus M, Suchet C, Thebaud C, Vargas P. The evolutionary history of
943   *Antirrhinum* in the Pyrenees inferred from phylogeographic analyses. BMC
944   Evolutionary Biology. 2014;14(1):146.
945 75. Donaire-Barroso D, Rivera X. La salamandra común *Salamandra salamandra*
946   (Linnaeus, 1758) en el subcantábrico: Origen, dispersión, subespecies y zonas de
947   introgresión. Butlletí Societat Catalana de Herpetología. 2016;23:7-38.
948 76. Thielsch A, Knell A, Mohammadyari A, Petrusek A, Schwenk K. Divergent clades or
949   cryptic species? Mito-nuclear discordance in a *Daphnia* species complex. BMC
950   Evolutionary Biology. 2017;17(1):227.
951 77. Díaz-Rodríguez J, Gehara M, Marquez R, Vences M, Goncalves H, Sequeira F, et al.
952   Integration of molecular, bioacoustical and morphological data reveals two new
953   cryptic species of *Pelodytes* (Anura, Pelodytidae) from the Iberian Peninsula. Zootaxa.
954   2017;4243(1):1-41.
955 78. Díaz-Rodríguez J, Gonçalves H, Sequeira F, Sousa-Neves T, Tejedo M, Ferrand N, et al.
956   Molecular evidence for cryptic candidate species in Iberian *Pelodytes* (Anura,
957   Pelodytidae). Molecular Phylogenetics and Evolution. 2015;83:224-41.
958 79. Barbosa S, Pauperio J, Herman JS, Ferreira CM, Pita R, Vale-Goncalves HM, et al.
959   Endemic species may have complex histories: within-refugium phylogeography of an
960   endangered Iberian vole. Molecular Ecology. 2017;26(3):951-67.

961   80.   Noguerales V, Cordero PJ, Ortego J. Inferring the demographic history of an
962   oligophagous grasshopper: Effects of climatic niche stability and host-plant
963   distribution. Mol Phylogenet Evol. 2018;118:343-56.
964   81.   Canestrelli D, Bisconti R, Sacco F, Nascetti G. What triggers the rising of an
965   intraspecific biodiversity hotspot? Hints from the agile frog. Scientific Reports.
966   2014;4:5042.
967   82.   Dufresnes C, Nicieza AG, Litvinchuk SN, Rodrigues N, Jeffries DL, Vences M, et al. Are
968   glacial refugia hotspots of speciation and cyto-nuclear discordances? Answers from
969   the genomic phylogeography of Spanish common frogs. Molecular Ecology.
970   2020;29:986-1000.
971   83.   Domènech M, Crespo LC, Enguídanos A, Arnedo MA. Mitochondrial discordance in
972   closely related *Theridion* spiders (Araneae, Theridiidae), with description of a new
973   species of the *T. melanurum* group. Zoosystematics Evolution. 2020;96:159.
974   84.   Escoda L, Castresana J. The genome of the Pyrenean desman and the effects of
975   bottlenecks and inbreeding on the genomic landscape of an endangered species.
976   Evolutionary Applications. 2021.
977   85.   Recuero E, Garcia-Paris M. Evolutionary history of *Lissotriton helveticus*: Multilocus
978   assessment of ancestral vs. recent colonization of the Iberian Peninsula. Molecular
979   Phylogenetics and Evolution. 2011;60(1):170-82.
980   86.   Irwin DE. Phylogeographic breaks without geographic barriers to gene flow.
981   Evolution. 2002;56(12):2383-94.
982   87.   Godet C, Clauzel C. Comparison of landscape graph modelling methods for analysing
983   pond network connectivity. Landscape Ecology. 2021;36(3):735-48.
984   88.   O'Hanlon SJ, Rieux A, Farrer RA, Rosa GM, Waldman B, Bataille A, et al. Recent Asian
985   origin of chytrid fungi causing global amphibian declines. Science.
986   2018;360(6389):621-7.
987   89.   Bosch J, Fernández-Beaskoetxea S, Garner TW, Carrascal LM. Long-term monitoring
988   of an amphibian community after a climate change- and infectious disease-driven
989   species extirpation. Global Change Biology. 2018;24(6):2622-32.
990   90.   Bosch J. Sapo partero común (*Alytes obstetricans*). In: Pleguezuelos JM, Márquez R,
991   Lizana M, editors. Atlas y libro rojo de los anfibios y reptiles de España. Madrid,
992   Spain: Dirección General de Conservación de la Naturaleza-Asociación Herpetologica
993   Española; 2002. p. 82–4.
994   91.   McKnight DT, Schwarzkopf L, Alford RA, Bower DS, Zenger KR. Effects of emerging
995   infectious diseases on host population genetics: a review. Conservation Genetics.
996   2017;18(6):1235-45.
997   92.   Cornuet JM, Ravigne V, Estoup A. Inference on population history and model
998   checking using DNA sequence and microsatellite data with the software DIYABC
999   (v1.0). BMC Bioinformatics. 2010;11:401.
1000   93.   Cabrera AA, Palsbøll PJ. Inferring past demographic changes from contemporary
1001   genetic data: A simulation-based evaluation of the ABC methods implemented in
1002   DIYABC. Molecular Ecology Resources. 2017;17(6):e94-e110.
1003   94.   Ebdon S, Laetsch DR, Dapporto L, Hayward A, Ritchie MG, Dincă V, et al. The
1004   Pleistocene species pump past its prime: Evidence from European butterfly sister
1005   species. bioRxiv. 2021.

1006   95.   Vences M, Hauswaldt JS, Steinfartz S, Rupp O, Goesmann A, Künzel S, et al. Radically
1007   different phylogeographies and patterns of genetic variation in two European brown
1008   frogs, genus *Rana*. Molecular Phylogenetics and Evolution. 2013;68(3):657-70.
1009   96.   Vences M, Sarasola-Puente V, Sanchez E, Amat F, Hauswaldt JS. Diversity and
1010   distribution of deep mitochondrial lineages of the common frog, *Rana temporaria*, in
1011   northern Spain. Salamandra. 2017;53:25-33.
1012   97.   Uy JAC, Borgia G. Sexual selection drives rapid divergence in bowerbird display traits.
1013   Evolution. 2000;54(1):273-8.
1014   98.   Polo-Cavia N, Oliveira JM, Villa AJR, Márquez R. Background colour matching in a wild
1015   population of *Alytes obstetricans*. Amphibia-Reptilia. 2016;37(3):253-60.
1016   99.   Evanno G, Regnaut S, Goudet J. Detecting the number of clusters of individuals using
1017   the software STRUCTURE: A simulation study. Molecular Ecology. 2005;14(8):2611-
1018   20.

1019

Supporting information

1020

1021 **S1 Fig. Summary of *A. obstetricans/almogavarii* samples incorporated into each**

1022 **main analysis.** (a) Geographic location of populations included in each analysis. For

1023 population codes see Fig 1. The inset map shows the distribution of the main

1024 lineages: orange - ND4 haplogroups E-F (*A. almogavarii*), yellow - ND4 haplogroup B

1025 (*A. o. obstetricans*), blue - ND4 haplogroup A (*A. o. pertinax*), red - ND4 haplogroup C

1026 (*A. o. boscai*), green - ND4 haplogroup D (*A. o. boscai*), black - unclear (adapted from

1027 Dufresnes and Martínez-Solano [23]). (b) Markers used in each analysis, with the

1028 corresponding number of samples and populations. Effective population sizes were

1029 calculated only for populations with ≥ 15 genotyped individuals. In the case of

1030 demographic history, only high mountain populations were included in the analysis.

1031

1032 **S2 Fig. Results of phylogenetic and clustering analyses for *Alytes***

1033 ***obstetricans/almogavarii*.** (a) Geographic distribution of the four mtDNA (ND4)

1034 haplogroups recovered in the analysis (blue: mtDNA haplogroup A, yellow: mtDNA

1035 haplogroup B, grey: mtDNA haplogroup E, orange: mtDNA haplogroup F). In four

1036 populations (T2, 61XR, BP and PI) we detected the presence of more than one

1037 haplogroup. (b) Results from Discriminant Analysis of Principal Components (DAPC)

1038 and (c) STRUCTURE for K = 7 microsatellite groups (see Fig 4). (d) Geographic

1039 distribution of the five genetic groups identified by microsatellite-based neighbour-

1040   joining analysis (see S7 Fig). White circles indicate populations with no data available

1041   for either ND4 or microsatellites. For population codes see Fig 1. The inset map

1042   shows the distribution of the main lineages: orange - ND4 haplogroups E-F (*A.*

1043   *almogavarii*), yellow - ND4 haplogroup B (*A. o. obstetricans*), blue - ND4 haplogroup A

1044   (*A. o. pertinax*), red - ND4 haplogroup C (*A. o. boscai*), green - ND4 haplogroup D (*A.*

1045   *o. boscai*), black - unclear (adapted from Dufresnes and Martínez-Solano [23]).

1046

1047   **S3 Fig. *Alytes* species tree produced in *BEAST based on one nuclear gene (β-**

1048   **fibint7) and four mitochondrial fragments (ND4, cyt-*b*, 12S and 16S).** Labels on

1049   branch tips correspond to the distinct ND4 haplogroups identified (blue: mtDNA

1050   haplogroup A, pink: mtDNA haplogroup B (central-western Pyrenean populations),

1051   yellow: mtDNA haplogroup B (Picos de Europa populations), grey: mtDNA haplogroup

1052   E, orange: mtDNA haplogroup F). Posterior probabilities of lineage divergence are

1053   indicated on branch labels.

1054

1055   **S4 Fig. Resulting plots from Discriminant Analysis of Principal Components (DAPC)**

1056   **across all *Alytes obstetricans/almogavarii* populations.** (a) Summary plots for K = 2-7

1057   genetic clusters. At K = 2, genetic clusters are represented as density curves. At K = 3-

1058   7, dots represent individuals and genetic clusters are shown as inertia ellipses.

1059   Legend labels indicate the different genetic clusters: eastern Pyrenees (EPY, orange),

1060   central Pyrenees (CPY, grey), central-western Pyrenees (CWPY, pink), Picos de Europa

1061   mountains (PEU, yellow), and Guadarrama Mountain Range (GUA, blue). (b)

1062   Distribution of BIC (Bayesian Information Criterion) values according to the number

1063   of clusters. The red arrow indicates the number of clusters chosen for DAPC analysis.

1064   The optimal number of clusters was assessed using the *find.clusters* function and

1065   determined as the K value above which BIC (Bayesian Information Criterion) values

1066   decreased substantially.

1067

1068   **S5 Fig. Results of Bayesian clustering analyses in STRUCTURE for microsatellites.** (a)

1069   Mean (± SD) log probability of the data [Ln Pr(XIK)] over 10 runs, for each value of K.

1070   (b) ΔK values as a function of K, calculated according to Evanno et al. [99].

1071

1072   **S6 Fig. Results of Tess3R analyses for microsatellites.** (a) Map depicting the

1073   distribution of ancestry coefficients inferred through Tess3R for K = 7 clusters. Black

1074   dots indicate the populations analysed. Colour codes as for STRUCTURE results. More

1075   saturated colours indicate a greater proportion of ancestry to either cluster. (b)

1076   Distribution of cross-validation scores according to the number of clusters. The red

1077   arrow indicates the number of clusters chosen for Tess3R analysis.

1078

1079   **S7 Fig. Neighbour-joining tree based on D_A distances for microsatellite markers.**

1080   Branch colours delineate the seven genetic clusters inferred by STRUCTURE (see Figs

1081   4a and 5), while colour shades around population codes correspond to the distinct

1082   mtDNA (ND4) haplogroups (blue: mtDNA haplogroup A, yellow: mtDNA haplogroup

1083   B, grey: mtDNA haplogroup E, orange: mtDNA haplogroup F; see Fig 3). In four

1084   populations (T2, 61XR, BP and PI) we detected the presence of more than one

1085   haplogroup. For population codes see S1 Table.

1086

1087   **S1 Table. Geographic information and standard genetic statistics of *Alytes***

1088   ***obstetricans/almogavarii* sampling localities.** Populations are grouped according to

1089   the genetic group of interest (EPY: eastern Pyrenees, CPY: central Pyrenees, CWPY:

1090   central-western Pyrenees, PEU: Picos de Europa mountains, GUA: Guadarrama

1091   Mountain Range). Lat. – latitude, Long. – longitude, Alt. – altitude in meters, N –

1092   sample size for microsatellites, Na – mean number of alleles, Ar – allelic richness

1093   standardized for sample size, H_O – observed heterozygosity, H_E – expected

1094   heterozygosity, F_{IS} – inbreeding coefficient, N_e – effective population size, N ND4 –

1095   sample size for ND4, ND4 haps – occurrence and code (in parentheses) of

1096   mitochondrial ND4 haplogroups identified in each population (see Fig 3), N cyt-b –

1097   sample size for cyt-*b*, N 12S – sample size for 12S, N 16S – sample size for 16S, N β-

1098   fibint7 – sample size for β-fibint7.

1099

1100   **S2 Table. Parameters used in DIYABC analysis and respective priors for the best**

1101   **supported scenarios.** The best supported scenarios were scenario 2 when

1102   considering only microsatellites (simple sequence repeats – SSRs) and scenario 5

1103   when including both mtDNA (ND4) and microsatellite markers. See Fig 2 for more

1104   information on tested scenarios. N – effective population size for each analysed

1105   deme (EPY – eastern Pyrenees; CPY – central Pyrenees; CWPY – central-western

1106   Pyrenees; PEU – Picos de Europa Mountains, GUA – Guadarrama Mountains), ra –

1107   admixture rate, t – time of events in generations (t_1 – time to the most recent split; t_2

1108   – time to the intermediate split; t_3 – time to the most ancient split). Microsatellite

1109   (SSRs) and mitochondrial (ND4) parameters: mean μ – mean mutation rate, individual

1110   locus μ – individual locus mutation rate, mean P – mean coefficient P, individual locus

1111 P – individual locus coefficient P, SNI – Single Nucleotide Insertion rate, mean k –

1112   mean coefficient k, individual locus k – individual locus coefficient k. Microsatellite

1113   loci were divided in two groups depending on the motif length (tri- and

1114   tetranucleotide loci). Conditions: sequence data were simulated under a Tamura Nei

1115   (TN93) mutation model.

1116

1117   **S3 Table. Microsatellite-based (below diagonal) and ND4-based (above diagonal)**

1118   **pairwise estimates of F_{ST} between the seven genetic groups identified by**

1119   **STRUCTURE in *Alytes obstetricans/almogavarii* (see Fig 5).** All P values < 0.01.

1120

1121   **S4 Table. Analysis of molecular variance (AMOVA) for mitochondrial (ND4) and**

1122   **nuclear (microsatellites) markers based on the seven genetic groups identified by**

1123   **STRUCTURE in *Alytes obstetricans/almogavarii* (see Fig 5).** All P values < 0.001.

1124

1125 **S5 Table. Posterior probability of tested scenarios and 95% confidence intervals (CI)**

1126 **estimated with DIYABC analysis when considering only microsatellites and when**

1127 **including both mtDNA (ND4) and microsatellite markers.** Type I and II errors for the

1128 best supported scenarios are indicated. See Fig 2 for more information on tested

1129 scenarios.

1130

1131 **S6 Table. Posterior parameters (median and 95% confidence intervals) and**

1132 **RMedAD (Relative Median Absolute Deviation) estimated with DIYABC analysis for**

1133 **the best supported scenarios when considering only microsatellites (simple**

1134 **sequence repeats – SSRs; scenario 2) and when including both mtDNA (ND4) and**

1135 **microsatellite markers (scenario 5).** See Fig 2 for more information on tested

1136 scenarios. N – effective population size for each analysed deme (EPY – eastern

1137 Pyrenees; CPY – central Pyrenees; CWPY – central-western Pyrenees; PEU – Picos de

1138 Europa Mountains; GUA – Guadarrama Mountains), ra – admixture rate, t – time of

1139 events in generations (t_1 – time to the most recent split; t_2 – time to the intermediate

1140 split; t_3 – time to the most ancient split), mean μ – mean mutation rate, mean P –

1141 mean coefficient P, mean k – mean coefficient k, $Q_{2.5}$ – quantile 2.5%, $Q_{97.5}$ – quantile

1142 97.5%.

1143

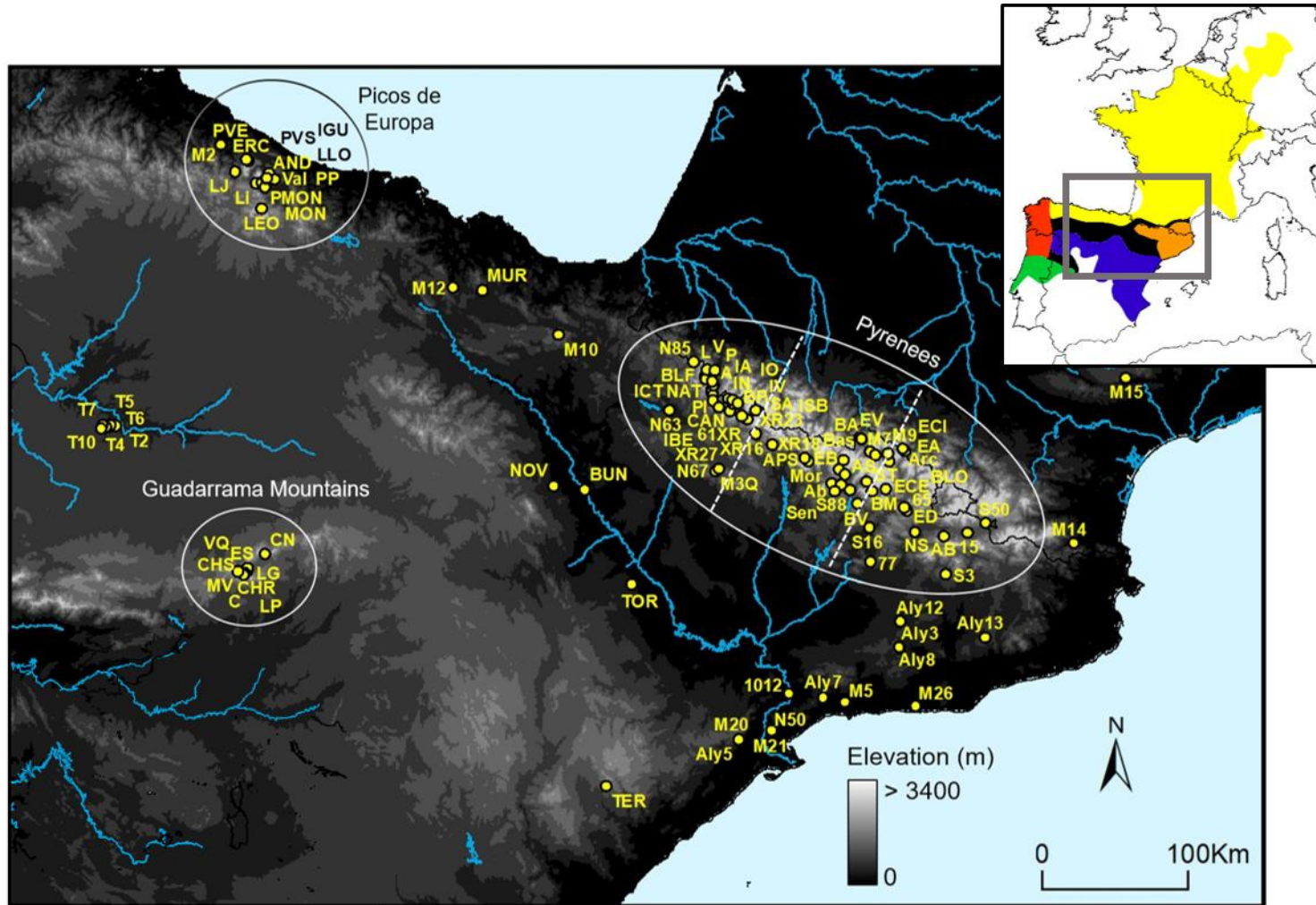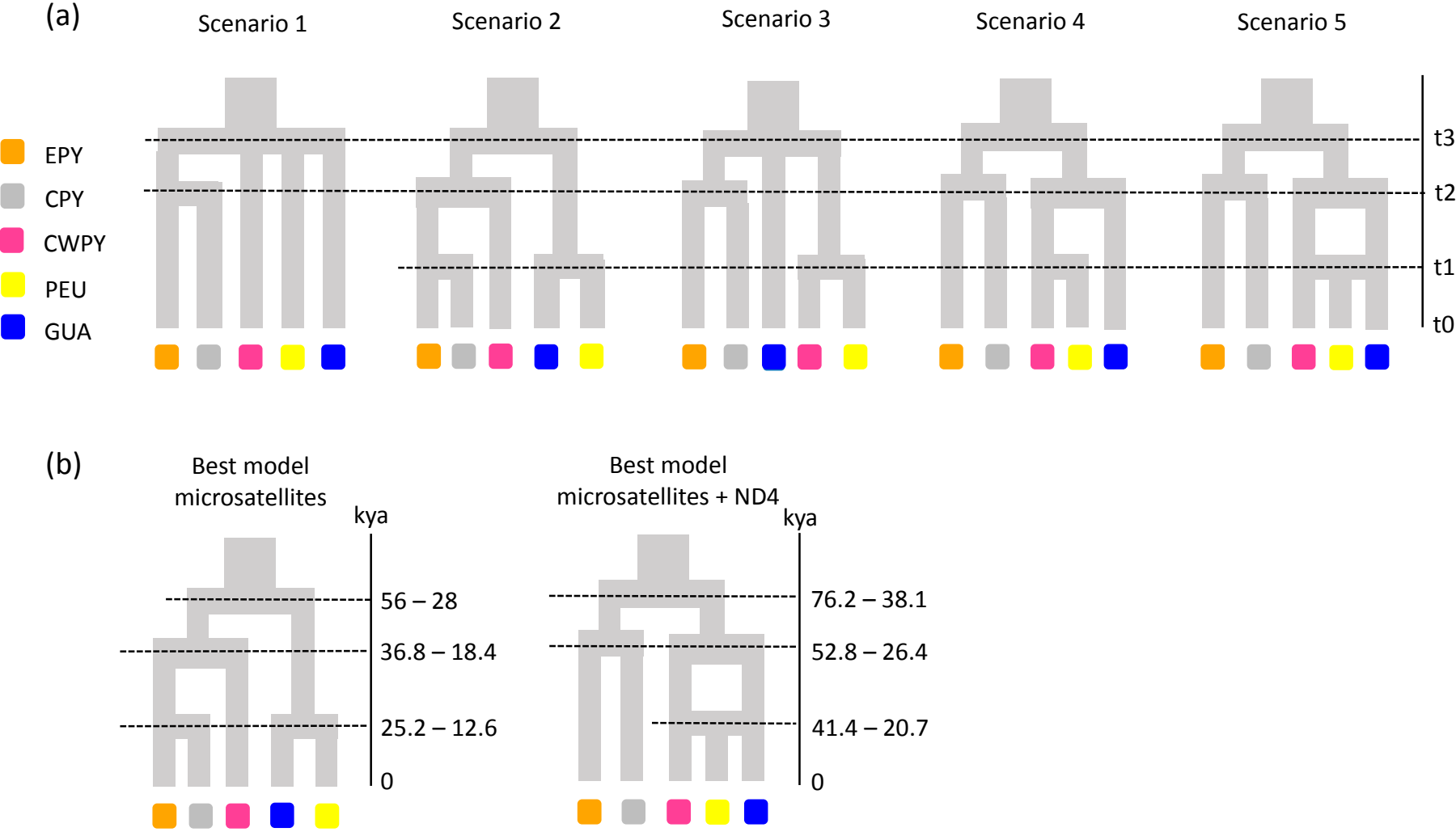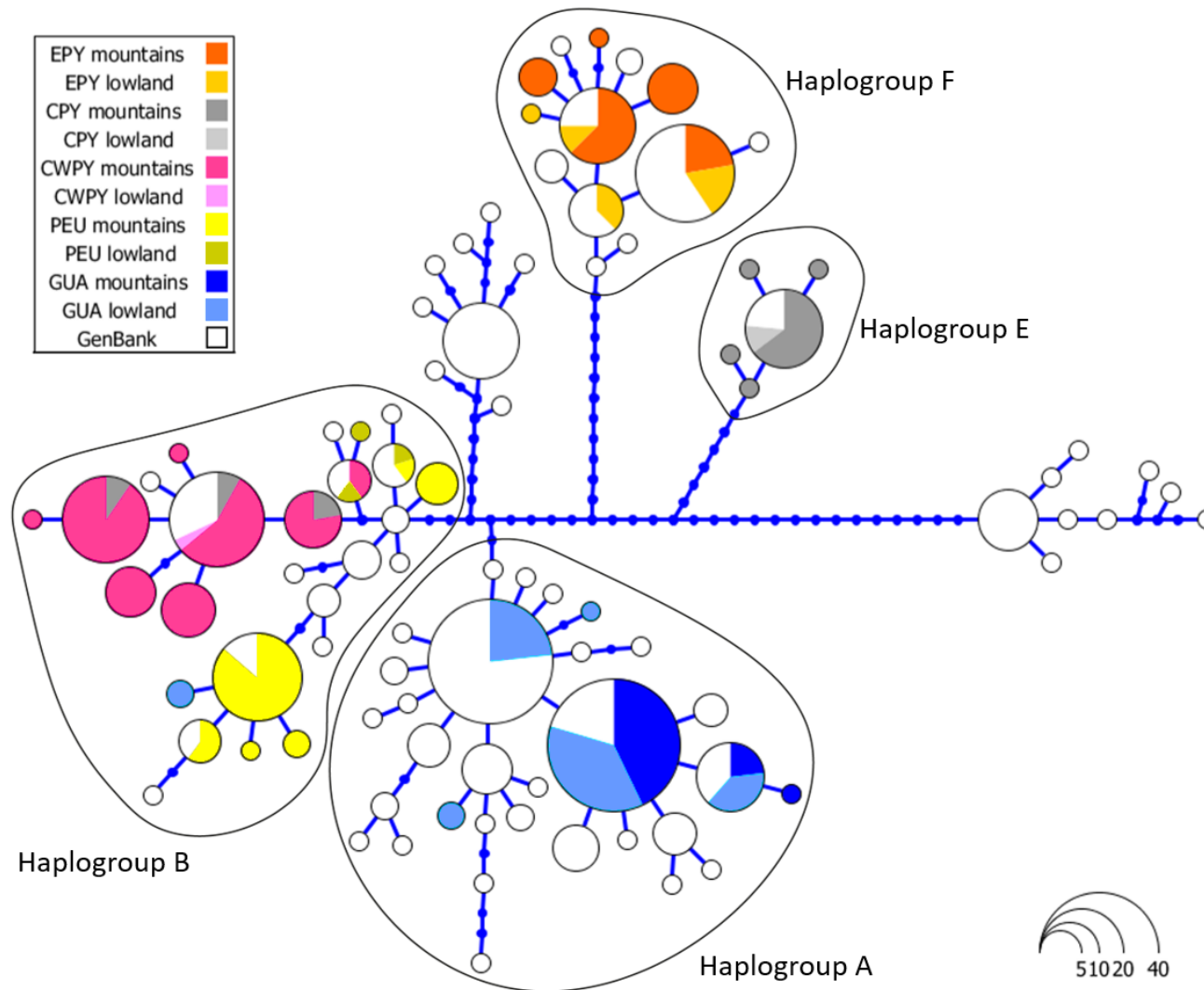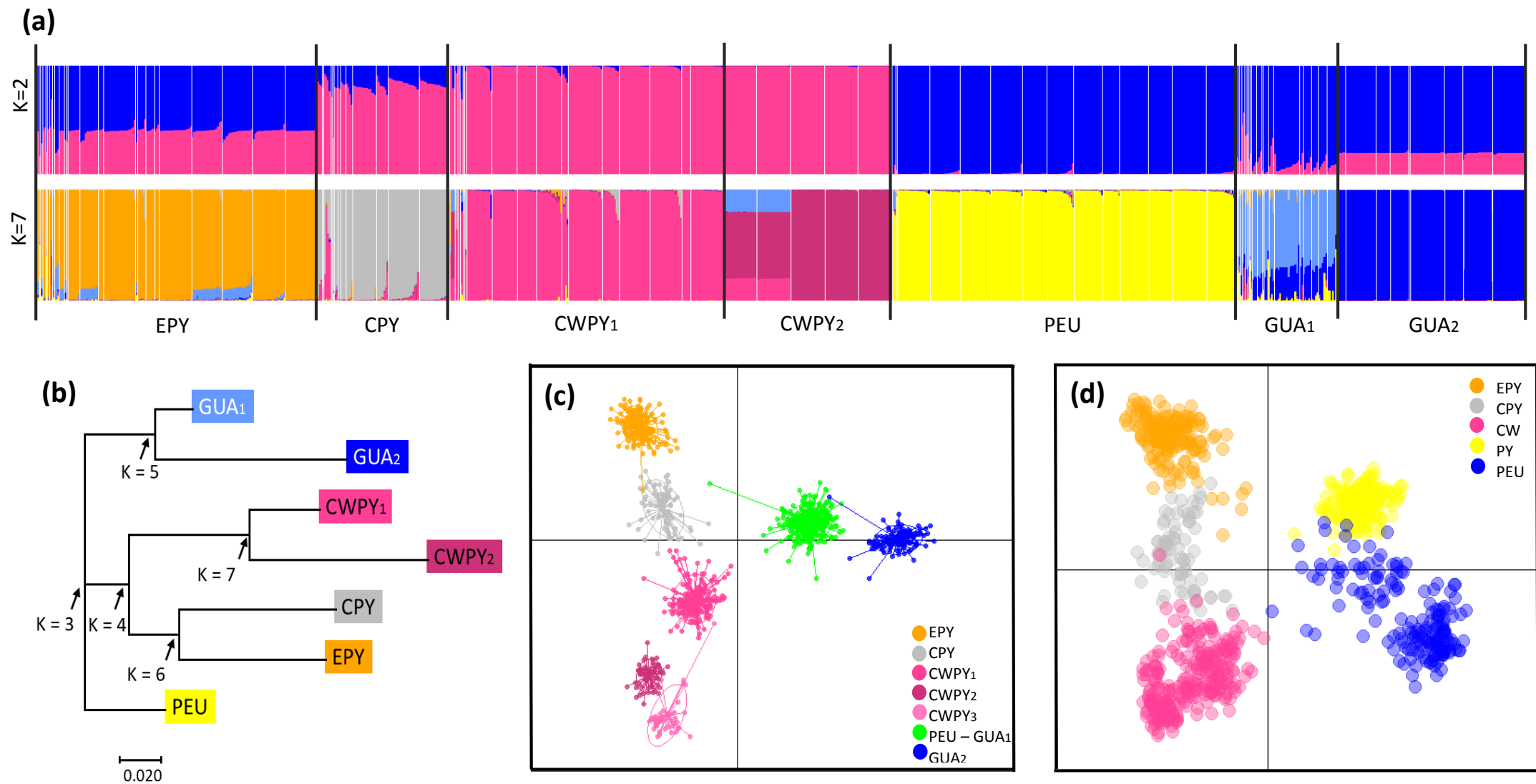1144 **S1 Appendix. Supporting methods.**

Fig 1

Fig 2

(a)

Scenario 1   Scenario 2   Scenario 3   Scenario 4   Scenario 5

EPY
CPY
CWPY
PEU
GUA

t3
t2
t1
t0

(b)

Best model
microsatellites

kya

56 – 28
36.8 – 18.4
25.2 – 12.6
0

Best model
microsatellites + ND4

kya

76.2 – 38.1
52.8 – 26.4
41.4 – 20.7
0

Fig 3

Fig 4

(a)

K=2

K=7

EPY CPY CWPY₁ CWPY₂ PEU GUA₁ GUA₂

(b)

GUA₁
GUA₂
K = 5
CWPY₁
CWPY₂
K = 7
CPY
EPY
K = 3
K = 4
K = 6
PEU

0.020

(c)

EPY
CPY
CWPY₁
CWPY₂
CWPY₃
PEU − GUA₁
GUA₂

(d)

EPY
CPY
CW
PY
PEU

Fig 5
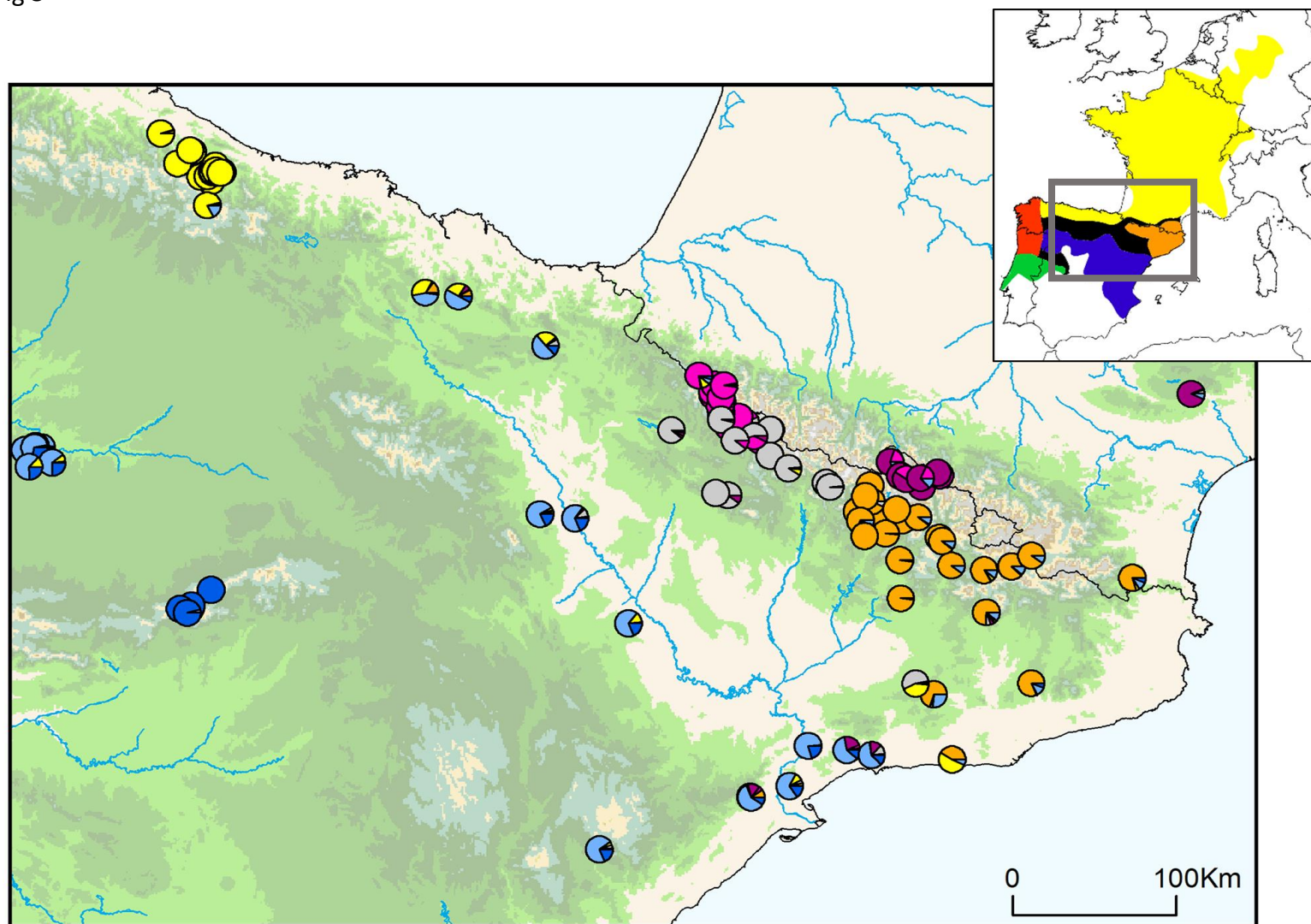
Fig 6

(a)

(b)
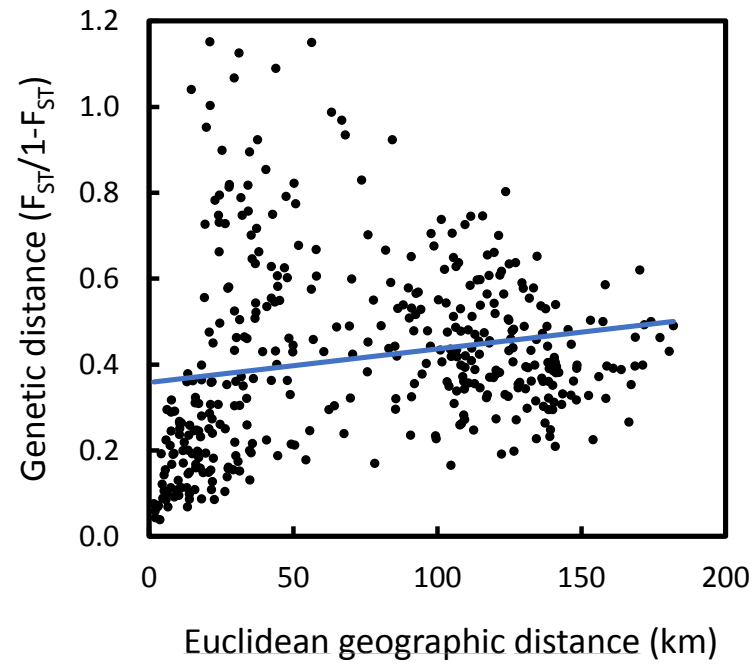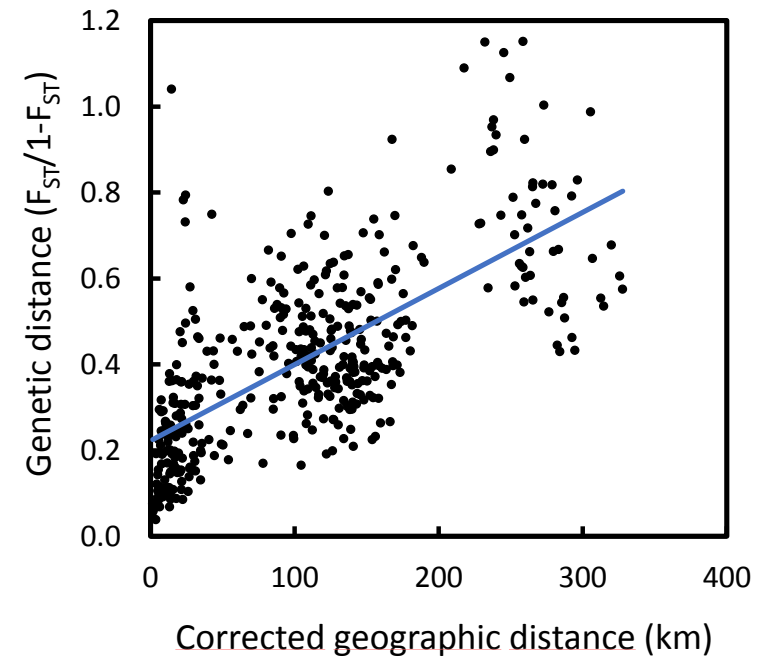
Click here to access/download
Supporting Information - Compressed/ZIP File Archive
Supporting information.zip